FATIGUE TESTS OF CRACKED AND REPAIRED ALUMINUM CONNECTIONS OF OVERHEAD SIGN STRUCTURES – FINAL REPORT

by

CHRIS P. PANTELIDES

JUSTIN NADAULD

August 2003

Civil & Environmental Engineering
College of Engineering
University of Utah
Salt Lake City, Utah

Report No.   CVEEN-03/2003

FATIGUE TESTS OF CRACKED AND REPAIRED ALUMINUM CONNECTIONS OF OVERHEAD SIGN STRUCTURES – FINAL REPORT

by

CHRIS P. PANTELIDES[1]

JUSTIN NADAULD[2]

[1]**Professor of Civil & Environmental Engineering**
[2]**Research Assistant**

Civil & Environmental Engineering
College of Engineering
University of Utah
122 South Central Campus Drive Rm 104
Salt Lake City UT 84112-0561

August 2003

ABSTRACT

Transportation departments have been using aluminum overhead sign structures since the early 1960's. It is well documented that cracks develop in the welds between diagonal and chord members due to fatigue stresses by wind-induced vibration of slender members from defect in the welds, during manufacture, or transportation to the site. The cracks propagate to complete failure of the members, which causes signs to fall and inflict injuries to roadway users. The original design of overhead sign structures did not consider fatigue as a limit state. In addition, field welding of aluminum structures for any possible repairs is prohibited. A repair method for the cracked aluminum welded connections between diagonal and chord members using glass fiber reinforced polymer composites (GFRP) is investigated.

The static tensile load carrying capacity and the fatigue limit of the welded connection and the cracked connection repaired with GFRP composites are established. The present report describes the surface preparation of the aluminum tubular members, the application sequence of the GFRP composite to retrofit the connection, and the experimental results from static and fatigue tests. The results from monotonic static tests carried out on repaired cracked welded specimens from actual sign structures show that the retrofitted connection achieved 1.17 to 1.25 times the capacity of the uncracked aluminum welded connection. The results from fatigue tests show that the repaired specimens with GFRP performed as well in fatigue resistance as the original aluminum welded specimens without cracks. The results of this study, along with the minimal traffic disruption anticipated in the field application, establish this retrofit method as a good candidate for implementation.

FORWARD

University of Utah Professor Chris P. Pantelides obtained a research grant from the New York State Department of Transportation (NYSDOT) and the Utah Department of Transportation (UDOT) for performing a research study regarding the fatigue evaluation of aluminum connections, both cracked and uncracked, of overhead sign structures. In addition, the fatigue evaluation of repaired aluminum connections with glass fiber reinforced polymer composites was performed.

Principal investigator for the project was Professor Chris P. Pantelides of the Department of Civil and Environmental Engineering. Justin Nadauld, graduate student at the Civil and Environmental Engineering Department, and Oliver Burt, undergraduate student at the Civil and Environmental Engineering Department, were the research assistants for the project.

This document constitutes the Final Report for the project. The NYSDOT manager for the project was Harry White, P.E., and the UDOT manager for the project was Doug Anderson, P.E.

ACKNOWLEDGEMENTS

TABLE OF CONTENTS

LIST OF FIGURES

LIST OF TABLES

1. Introduction

Overhead sign structures support signs that make travel safer by providing timely information to the driver. However, several aluminum sign structures after inspection exhibit structural damage, the most prevalent of which is cracking of the joint between internal trussing and the main chords. The cause of the cracks is due to several factors, the greatest contributor of which is the fact that when the original truss designs were done in the 1960's fatigue design was not a code requirement. Other factors include lack of shop inspection during fabrication, insufficient construction supervision, and thermal strains developed in the welding process, all of which may cause internal stresses into the overhead sign structure before the sign is attached. Cracks in the welds of aluminum overhead sign structures can propagate to complete failure of members, which can cause signs to fall and cause injuries. The truss considered here is a three-dimensional truss, or tri-truss system, as shown in Figure 1. Figure 2 shows a typical crack in a welded aluminum connection.
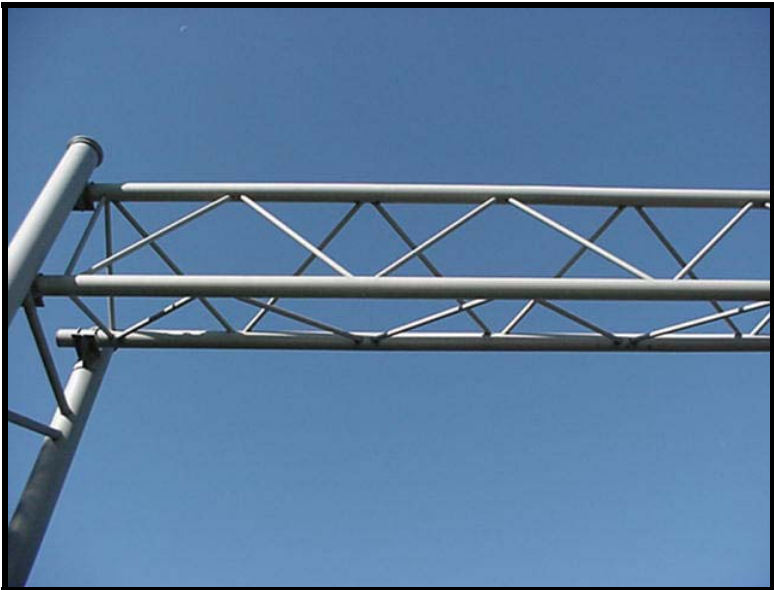
Figure 1. Tri-truss aluminum overhead sign support structure

Figure 2. Crack through aluminum-welded joint of overhead sign structure

A repair method for cracked aluminum welded connections of overhead sign structures using glass fiber reinforced polymer GFRP composites had been investigated previously (Pantelides and Nadauld 2001). The tests performed in that investigation consisted of pulling the diagonal members from the joint with the chord member in monotonic static tension. The as-is aluminum welded connection without any visible cracks was able to resist a stress of 14.0 ksi or 1.16 times the allowable stress for welded tubes according to the *Aluminum Association Specifications* (1986). The GFRP composite retrofitted field connections with cracks in the welds, which ranged from ¼ to $^2/_3$ of the total weld length, reached static monotonic tensile stress capacities of 16.4 ksi to 17.45 ksi, which constitutes a ratio of 1.17 to 1.25 times that of the as-is welded connection with no visible cracks. The experimental results of that study had demonstrated that the method developed was a viable repair technique for cracked welded connections of aluminum sign structures.

The present research targets the fatigue life of the as-is connections without any visible cracks, and that of the retrofitted connections with GFRP composites. This is important for determining how many cycles to failure the retrofitted connection with GFRP composites can tolerate. The tests carried out in this research also provide fatigue information about the as-is welded connections, which were obtained from the field in two conditions: (a) cracked condition, (b) uncracked condition. The uncracked connections were tested to determine the fatigue life of the as-is aluminum connections in the field. The cracked connections were also obtained from the field; they were retrofitted with GFRP composites and then subjected to identical fatigue tests as the uncracked aluminum connections. In addition, new aluminum connections were fabricated by tack-welding the aluminum tubes; the tack welds were applied at only four points to form the geometry, and the joints were wrapped to form an all-composite GFRP connection. These connections form the third series of fatigue tests. Finally, four tests using test units obtained from the field with the weld 90% destroyed were performed. These tests were added due to the poor performance of the new tack-welded aluminum tubes, caused by poor bonding of the FRP to new aluminum that had not oxidized. The report provides comparisons between the number of cycles to failure of the as-is uncracked specimens and the retrofitted specimens with GFRP composites; it is believed that these comparisons can provide engineers useful information about the expected life of the retrofitted connections.

2. Objectives

The overall objective of the present study is to investigate the performance of the as-is and retrofitted aluminum connections with GFRP composites under fatigue loads. The aluminum connections were subjected to constant amplitude fatigue tests at three stress ranges and at a fixed frequency of 2 Hz. The ultimate goal is to determine the strength of the as-is and retrofitted connection after it has withstood fatigue loading at various stress ranges up to 1×10^6 cycles and the remaining static load capacity after this number of cycles if the connection reaches 1×10^6 cycles. In addition to the fatigue tests, two additional static tests for uncracked aluminum joints from the field were performed to establish the static load capacity of the as-is joints. Analytical models of a typical tri-truss bridge structure are investigated for various cases including damaged due to cracks, as well as repaired with GFRP composites.

3. Sign Structure and Sign Structure Elements

Sign Structure

Currently there are several types of aluminum sign structures that are in service throughout the United States. In this study the tri-truss structure, as shown in Figure 3, has been used as the prototype. This type of structure has been extensively used by the NYSDOT throughout their infrastructure, with thousands of such structures in service today. However, although this study focuses on the tri-truss, the procedures and results outlined in this report could be easily extended to other types of aluminum sign structures that have similar element sizes and geometries.

The tri-truss consists of chord and diagonal elements, as shown in Figure 3(c). The chord elements make up the three corners of the tri-truss. The diagonals span between the chord elements, as shown in Figure 3(a). The connections between the diagonals and the chords are typical K connections, with an angle θ between 35 and 60 degrees. In the testing presented in this paper the angle θ was within the range of 42 to 48 degrees. All of the diagonal-chord connections are all around fillet welds, with a minimum throat equal to the thickness of the diagonal element. This connection is the primary focus of this report, and will be denoted as a sign structure element, as shown in Figure 3(a).

Two main types of supports have been used to support the tri-truss, a single steel post or a trussed post. Figure 3(d) shows a typical single post support; this support type was used when modeling the structure in Section 7 - Analytical Model. The trussed post support consists of two posts, one to support the two chords that are in the same vertical plane, and a second post to support the third chord. The two posts are connected using web members. All of the posts used are typically ASTM A572 Grade 60 steel with various diameters, depending on post height and truss span length.

The posts are supported on circular or rectangular concrete footings, and are anchored to the footing with 4 anchor bolts, as shown in Figures 3(a), (b), and (d). The concrete footings vary in plan dimensions and height, according to the specified loads.

The sign structures vary in the number and size of signs they support. For purposes of the analytical portion of this study, the signs shown in Figure 3(a) were used. It is important to note that all of the test results are based on the performance of a single sign structure element and, therefore, the test results are not affected by the number or size of the signs, the span of the truss, the height or type of posts, or the size or depth of footings used. These parameters are only important for use in the analytical study of the sign structure, and are not intended to limit the scope of this research. The emphasis in this study was to compare ultimate strengths of as-is (Aluminum) and repaired joints (GFRP).

78'

19'-3" 15'-6" 8'-6" 15'-6" 19'-3"

1'-3" B 1'-3"

4' 4'

B

9'-6" 8'-6"

Typical Sign Structure Element

4

22'-3" 22'-3"

A A

9' 9'
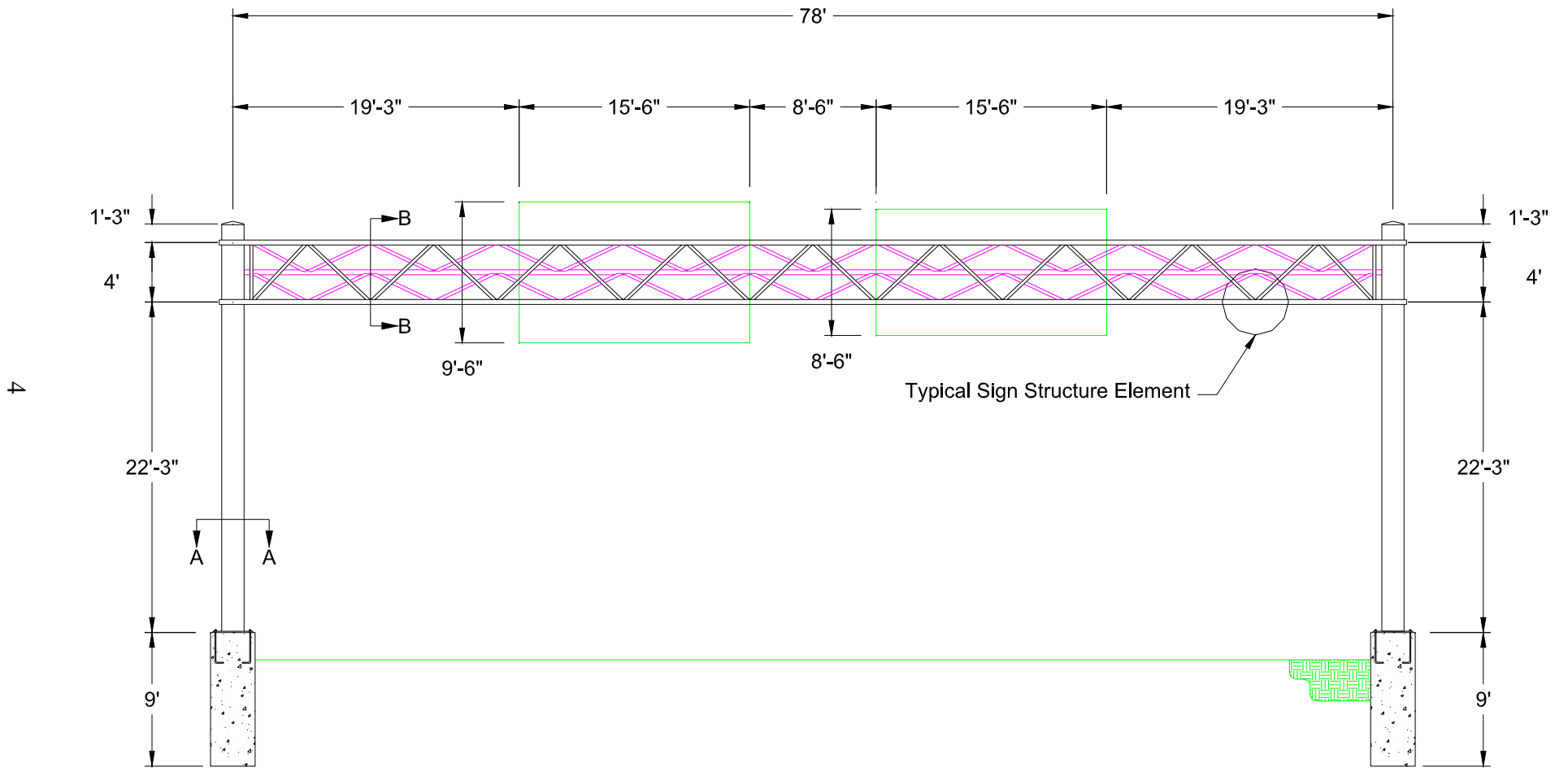
ELEVATION - FRONT VIEW
(a)

Figure 3. Typical sign structure

Concrete Footing

Steel Base Plate

457mm (18in.) DIA.
Steel Pipe

Anchor Bolt

SECTION A-A

(b)

$3'-5\frac{1}{2}"$

4'

Chord Element

Branch Element

SECTION B-B

(c)

1'-3"

4'

22'-3"

9'
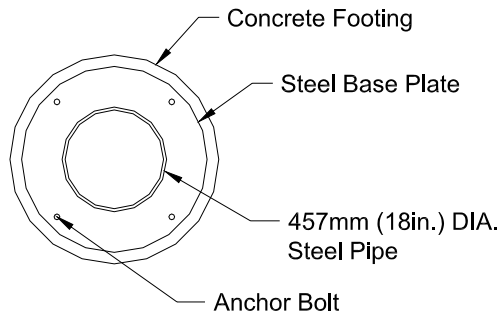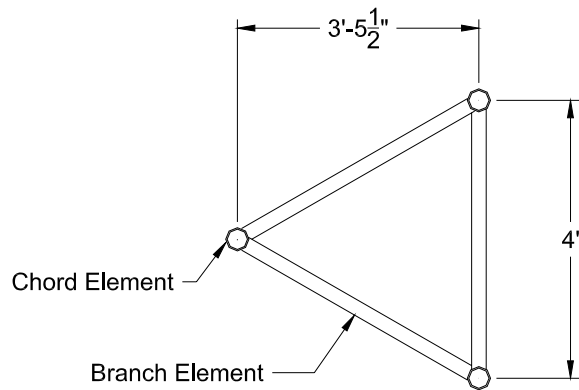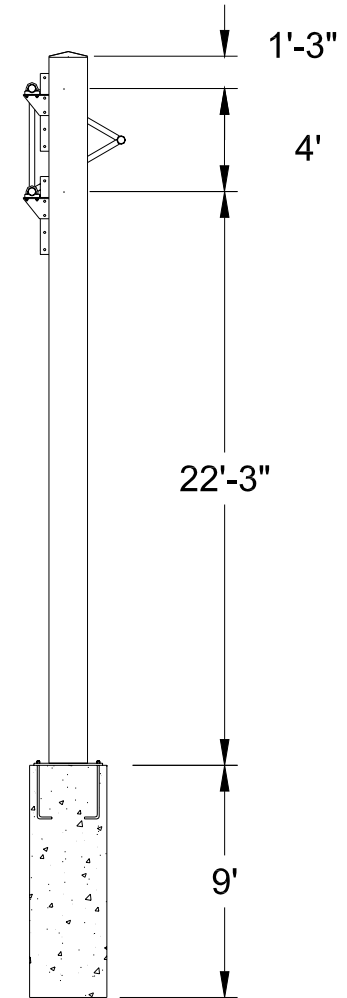
ELEVATION - SIDE VIEW

(d)

5

Figure 3 (cont.). Typical sign structure

Sign Structure Elements

The sign structure elements (or test units) consisted of two diagonal members to a main chord; the diagonals are orientated at between 42 and 48 degrees from the chord as shown in Figure 4. All of the test units are of the same geometry and outer dimensions, allowing them to be tested in the same loading frame.

The members of the sign structure element consist of round aluminum tubing with the dimensions for the diagonals and chord members as shown in Table 1. The two types of aluminum tube dimensions were used in a random manner, based on the limited number of test units available. These types are distinguished as Type I or Type II, as shown in Table 1. It should be noted that these sizes are typical for diagonal and chord members of overhead highway sign structures; however, depending on the span of the structure, truss depths ranging from 4-ft to 8-ft, diagonals ranging from 1½ in. to 5 in. outside diameter, and wall thickness ranging from $^1/_8$ in. to ¼ in. are available (NYSDOT 1968).

In order to apply a monotonic static or dynamic tensile load, a triangular load frame was constructed such that one diagonal of the specimen could be positioned vertically, directly under the hydraulic actuator as illustrated in Figure 4. For the dynamic testing (fatigue testing) the triangular load frame was fitted with lateral bracing as shown in Figure 5. These braces were provided for additional stiffness to withstand the dynamic loading effects. For the majority of the fatigue tests a steel tube was placed inside the aluminum chord. This was to stiffen the chord and minimize bending stresses induced in the chord caused by the test setup – see Figure 3. This situation better represents the in service condition, where the second diagonal would resolve the vertical force and only a small amount of bending stress would be induced into the chord.

LOAD

GRIPPING MECHANISM

ALUMINUM TUBE
4 in. O.D.

ALUMINUM TUBE
2.5 in. O.D.

48 °

24 in.

FILLET
WELD

BOLTED
SUPPORTS

W 10 x 49

W 10 x 49

W 10 x 49

W 10 x 49

51.5 in.

48 in.

72 in.
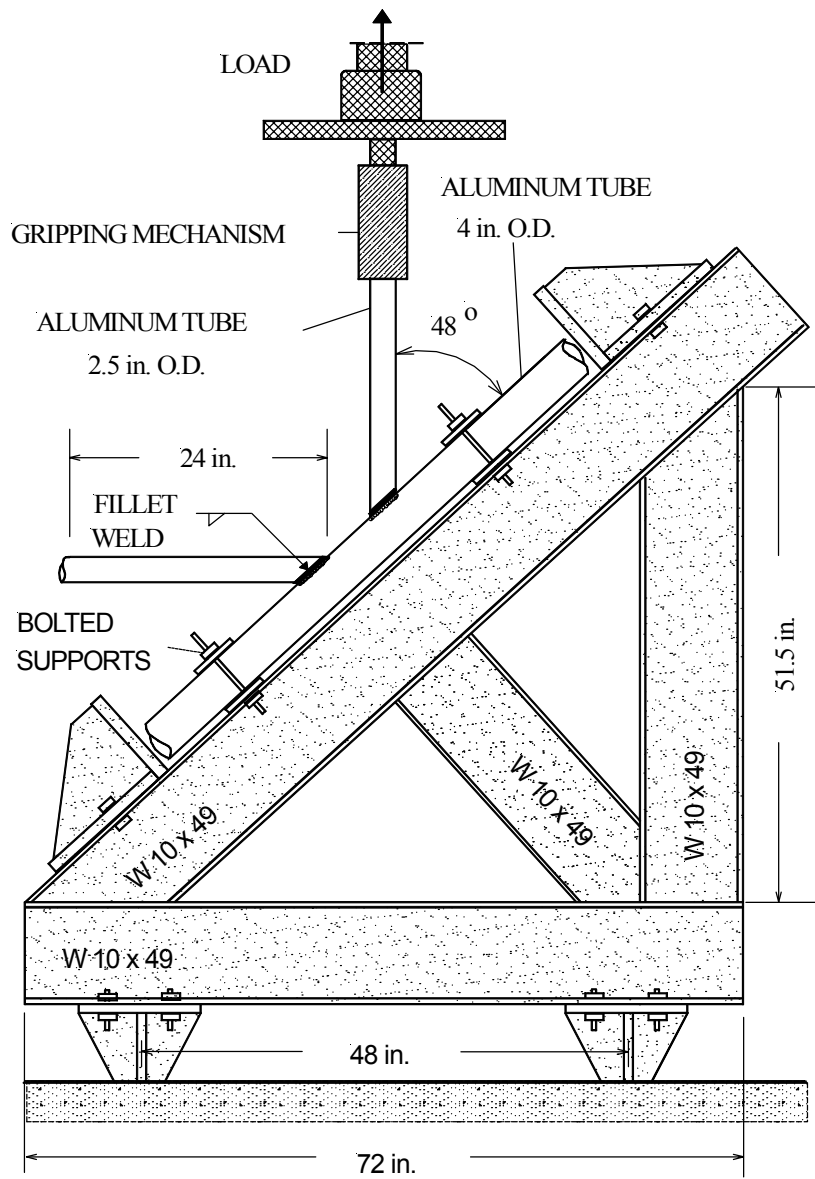
Figure 4. Support frame and test configuration

Table 1. Aluminum Tube Dimensions

	Pipe (1)	O.D. (in.) (2)	I.D. (in.) (3)	Thickness (in.) (4)	Area (in.^{2}) (5)
TYPE I	Diagonals	2 ½	2	¼	1.767
	Main Chord	4	3 ½	¼	2.945
TYPE II	Diagonals	2 ½	2 $^1/_8$	$^3/_{16}$	1.362
	Main Chord	4	3 ½	¼	2.945

Figure 5. Lateral bracing used for dynamic testing

4. Technique

NYSDOT provided twelve field collected sign structure elements for performing the fatigue tests with dimensions shown in Table 1; of these, six were uncracked sections and six cracked sections. Two of the six uncracked sections were provided by NYSDOT to perform two static tension tests following the procedures described in the completed investigation (Pantelides and Nadauld 2001). Seven tack-welded aluminum specimens were provided by Air Logistics Corporation for a series of fatigue tests on GFRP retrofitted specimens; these specimens were intended to demonstrate the fatigue strength of the connection with only the GFRP composite contribution. This series was expected to produce the true strength of the GFRP connection after fatigue loading at various stress ranges, since there was no strength offered by the aluminum weld. However, it was determined that these tests did not perform as expected due to a significant decrease in bond strength caused by the use of new aluminum tubes for the test units. Therefore, two additional tests were performed using reclaimed aluminum sections, with the weld 90% destroyed. These tests were expected to produce the true strength of the GFRP connection in the field when the retrofitted joint has been completely severed.

Two types of tests were performed in this research: static and fatigue tests as described below. The static tests were for two aluminum truss specimens from the field, and constitute tensile tests to failure (Series I). The fatigue tests were of three types: (Series II) as-is aluminum truss specimens from the field with no visible cracks, (Series III) cracked aluminum truss specimens from the field retrofitted with GFRP, (Series IV) tack-welded aluminum specimens retrofitted with GFRP, and (Series V) aluminum truss specimens from the field with the weld 90% destroyed and retrofitted with GFRP.

Series (I): Static Tests

Two tests of uncracked specimens to failure were performed. One test had been performed in a previous study (Pantelides and Nadauld 2001); two additional tests were performed in order to determine the average static tension capacity of the uncracked joints using three tests. However, the failure modes and geometry of the two new tests were different from those of the first test, as shown in Table 1. Therefore only the two recent tests were used to determine the average static tension capacity of uncracked joints. The tests were performed in the existing fixture as shown in Figure 4.

The results of the two static tests were as follows:

Test I(a): Tensile failure load = 28.8 kips
Test I(b): Tensile failure load = 28.3 kips

The average static tensile load carried by the uncracked aluminum joint is evaluated as 28.6 kips.

Series (II): Fatigue Tests of As-is Welded Aluminum Connections with No Visible Cracks

Fatigue failure of aluminum overhead sign structures may occur during fabrication, transportation to the site, erection, operation, or service. Several examples exist of fatigue failures not caused by operating loads but rather by cyclic loads that occurred during their shipment to the site. A large percentage of fatigue cracks are caused by wind-induced vibration of members that are too slender (Sharp et al. 1996). Repair of welded aluminum connections in the field is generally not recommended because of the difficulty in maintaining the gas enclosure over the arc in the wind. For repair of cracks in groove-welded plate specimens using welds, it has been noted that even though good practice was employed in making the repairs, the geometry of the bead, the quality of the weld, and the fatigue life were generally not as good as those of the original joint (Sharp et al. 1996).

Fatigue data on failure of welded joints in tubular aluminum trusses show that such failures can be calculated using the total applied stress at the edge of the weld, that is, the axial and bending stress in the member added to the stress from local bending of the tube wall. To obtain these stresses, a finite element analysis of the truss must be made. The fatigue failure in tests for welded joints in tubular aluminum trusses occurred in the range of 10,000 to 2 million cycles, depending on the level of maximum stress range (Sharp 1993).

The 1975 edition of the *Standard Specifications for Structural Supports for Highway Signs, Luminaires and Traffic Signals* (AASHTO 1975) suggests that sound practice in designing highway signs should be based on the infinite life (endurance limit) of the materials. This generally represented the 2 million-cycle failure stress for steel, and the 500-million-cycle failure stress for aluminum. However, it should be noted that these figures represent welds of new structures without fatigue cracks. In the 1996 AASHTO *Standard Specifications*, the constant amplitude fatigue threshold was termed the allowable fatigue stress range for more than 2 million cycles on a redundant load path structure (AASHTO 1998). The fourth edition of the *Standard Specifications for Structural Supports for Highway Signs, Luminaires and Traffic Signals* (AASHTO 2001) adopts an infinite life design approach for fatigue design criteria. This is considered sound practice and is generally based on the Constant Amplitude Fatigue Limit (CAFL) as shown in Table 2.

Table 2. Constant Amplitude Fatigue Threshold

Detail Category	Aluminum Threshold (ksi)
A	10.2
B	6.0
B'	4.6
C	4.0
D	2.5
E	1.9
E'	1.0
ET	0.44
K_2	0.38

Details provided in the fourth edition of the *Standard Specifications for Structural Supports for Highway Signs, Luminaires and Traffic Signals* (AASHTO 2001) classify the joint under investigation as Detail 19 (Example 10) fillet welded T-, Y-, and K-tube–to-tube connection for which the stress category with respect to stress in the chord is Category E. Using an area of 1.767 in^2 for the diagonal brace member gives an applied load of 3.4 kips for the load corresponding to the CAFL threshold.

The University of Utah has a 220 kip programmable actuator, which was used to perform fatigue strength studies of carbon FRP retrofitted concrete bridge decks with corroded rebar. The present tests were performed in the same fixture as shown in Figures 4 and 5. From measurements of vibration on actual aluminum highway sign structures, the range of fundamental frequencies ranges from 0 to 5 Hz. The frequency of the fatigue cycles used in the present tests was 2 Hz, i.e., two cycles per second. The definition of the terms maximum stress, minimum stress, mean stress, stress range, and stress ratio is also given in Figure 6.
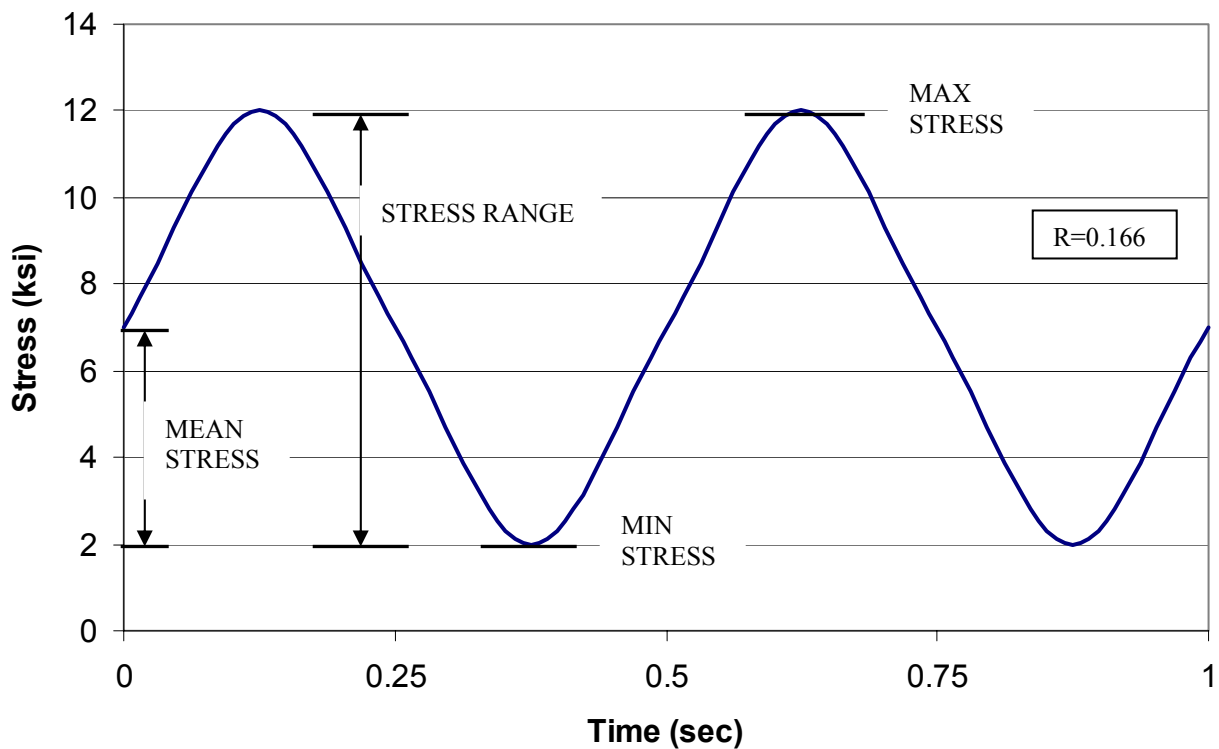
Figure 6. Constant amplitude fatigue test

It should be noted that the minimum stress that will be used in the tests is higher than zero, as shown in Figure 5. The stress ratio R = (min. stress / max. stress) used in the tests was close to R = 0.20. In Figure 6 the value of the stress ratio is R = $^2/_{12}$ = 0.166.

In the present tests, the maximum number of cycles was limited to 1x10^6 cycles, followed by a static test if the joint had survived the 1x10^6 cycles. The maximum number of cycles is significant, since 1x10^6 cycles is equivalent to 100 cycles per day, every day for approximately 27.4 years. Many of the actual specimens were obtained from trusses that were in service for a number of years, therefore the additional 1x10^6 cycles were considered sufficient. Considering the approach taken in the NCHRP Report 412 (Kaczinski et al. 1998), the 37-mph-gust speed

correlates to a 0.01% exceedance for a yearly mean wind velocity of 11 mph. The 37-mph-gust speed also correlates to the hourly mean velocity, i.e. wind speed that occurs on average one hour each year. It will be shown in Section 7 that the sign truss considered has a fundamental frequency of 3.33 Hz. For an area where the yearly mean wind speed is 11 mph, the number of 37-mph gust stress cycles per year is:

$$0.0001 \times 365 \times 24 \times 3600 \times 3.33 = 10,500 \text{ cycles/year}$$

that shows that the 1×10^6 cycles would represent approximately 95 years, which is longer than the remaining life of the structure. The static test following the 1×10^6 fatigue cycles represents the remaining life of the joint. Given the above information, the test series shown in Table 3 was used for fatigue testing of as-is welded aluminum connections with no cracks.

Table 3. Test Matrix for Fatigue Tests of As-is Welded Aluminum Connections With No Visible Cracks

Specimen	Condition	Source	Test	Stress (ksi)
II-a	Uncracked	NYSDOT	Cycle to failure at 21 kips	12.0
II-b	Uncracked	NYSDOT	Cycle to failure at 15 kips	8.5
II-c	Uncracked	NYSDOT	Cycle to failure at 10 kips	5.7
II-d	Uncracked	NYSDOT	Cycle to failure at 6 kips	3.4

In Table 3, the upper stress level is 21 kips, which corresponds to a stress of 12 ksi and is 85% of the ultimate strength of the static test performed in the earlier study (Pantelides and Nadauld 2001), and 73% of the Series (I) test results carried out in the present study. Note also that this stress is higher than the Detail Category A stress of Table 2 recommended in AASHTO (2001), by a factor of 1.17. The lower bound stress level is 6 kips, at a stress of 3.4 ksi, which is 1.79 times the Constant Amplitude Fatigue Threshold of Table 2 for Detail Category E. However, it should be noted that Table 2 refers to design criteria, which are conservative, as opposed to Table 3, which draws upon the experience from actual test results. The four stress levels of 3.4 ksi, 5.7 ksi, 8.5 ksi and 12 ksi provide a large enough spread so that a good distribution of stress range versus number of cycles to failure can be obtained.

Series (III): Fatigue Tests of Cracked Aluminum Connections from the Field Retrofitted with GFRP

The test series shown in Table 4 was used for fatigue testing of cracked aluminum connections from the field retrofitted with GFRP.

Table 4. Test Matrix for Fatigue Tests of Cracked Aluminum Connections From the Field Retrofitted With GFRP

Specimen	Condition	Source	Test	Stress (ksi)
III-a	Cracked/GFRP wrapped	NYSDOT	Cycle to failure at 21 kips	12.0
III-b	Cracked/GFRP wrapped	NYSDOT	Cycle to failure at 15 kips	8.5
III-c	Cracked/GFRP wrapped	NYSDOT	Cycle to failure at 10 kips	5.7
III-d	Cracked/GFRP wrapped	NYSDOT	Cycle to failure at 6 kips	3.4

In Table 4, the upper stress level is 21 kips, which corresponds to a stress of 12 ksi. This is the same as that of the as-is uncracked specimens of Series (II). The same strategy is used as for Series (II) regarding the remaining three test units.

Series (IV): Fatigue Tests of Tack-welded Aluminum Connections Retrofitted with GFRP

The test series shown in Table 5 was used for fatigue testing of tack-welded new aluminum connections retrofitted with GFRP. This series was expected to produce the true strength of the GFRP connection after fatigue loading at various stress ranges, since there would be no strength offered by the weld. However, it was determined that these tests did not perform as well as expected due to decreased bond strength when bonding to new aluminum pipes. The same strategy is used as for Series (II) regarding the remaining two test units.

Table 5. Test Matrix for Fatigue Tests of Tack-welded Aluminum Connections Retrofitted With GFRP

Specimen	Condition	Source	Test	Stress (ksi)
IV-a	GFRP wrapped	Air Logistics	Cycle to failure at 21 kips	12.0
IV-b	GFRP wrapped	Air Logistics	Cycle to failure at 15 kips	8.5
IV-c	GFRP wrapped	Air Logistics	Cycle to failure at 10 kips	5.7

Series (V): Fatigue Tests of Reclaimed Aluminum Connections with the weld 90% destroyed and Retrofitted with GFRP

The test series shown in Table 6 was used for fatigue testing of aluminum connections from the field with the weld 90% destroyed and retrofitted with GFRP. This series was expected to produce the true strength of the GFRP connection after fatigue loading at various stress ranges, since there would be no strength offered by the weld. Also, the aluminum used was from the field, therefore a good bond was expected without the issues faced in Series (IV). The same strategy is used as for Series (II) regarding the remaining three specimens.

Table 6. Test Matrix for Fatigue Tests of Aluminum Connections from the Field with the weld 90% destroyed and Retrofitted with GFRP

Specimen	Condition	Source	Test	Stress (ksi)
V-a	GFRP wrapped	NYSDOT	Cycle to failure at 21 kips	12.0
V-b	GFRP wrapped	NYSDOT	Cycle to failure at 10 kips	5.7
V-c	GFRP wrapped	NYSDOT	Cycle to failure at 6 kips	3.4

13

5. Experimental Results

This chapter describes the experimental results obtained in both the static and fatigue load tests described in the previous section. The results of the static testing were obtained following the procedure outlined in the previous study (Pantelides and Nadauld 2001). The results of the fatigue tests were obtained using two data acquisition and control systems: the MTS TestStar II system and the WIN5000 Measurements Group Data Acquisition system. The MTS system consists of a 220 kip programmable actuator that was used to apply a constant force amplitude tensile load to the test units as shown in Figures 4 and 5. The load was applied at a constant frequency of 2 Hz. The load, displacement, and time for each test were recorded at every peak and valley. The WIN5000 Measurements Group Data Acquisition system was used to record the strain from strain gages placed on the specimens. Strain data was recorded at two different time intervals. The first tests were recorded at 0.1-second intervals. This interval was found to be too long for the 2 Hz loading, and as a result the peak strains were not consistently recorded. The remaining tests were recorded at 0.04-second intervals (25 scans per second) for two cycles (four seconds) every 600 cycles (five minutes). This recording interval resulted in more accurate records of the peaks and valleys.

The fatigue results are presented in three different plots – Load vs. Cycles, Displacement vs. Cycles, and Cumulative Damage vs. Cycles. The Load and Displacement curves were obtained directly from the output of the MTS TestStar II system, and they coincide with the load and displacement of the actuator. The Cumulative Damage is defined as follows:

$$D = 1 - \frac{k_i}{k_o}$$

Where

D = Cumulative Damage
k_i = Stiffness at Cycle (i), kips/in.
k_o = Initial Stiffness, kips/in.

The Cumulative Damage Index is a measure of the loss of stiffness of the test unit (sign structure element). This measurement is unitless and provides an effective way to compare results of the fatigue tests. The significance of D is that when its value is small and the unit reaches 1×10^6 cycles it means that the unit behaves well; however, when he unit fails early and the D index is small, this means that the unit failed with little displacement or warning.

Series (I) Results

Static tests I-a and I-b had a similar failure mode and load/displacement curve. Failure occurred at the toe of the weld and continued almost entirely around the chord, as can be seen in Figure 7. Immediately following failure of the chord the diagonal was subjected to combined tensile and bending stress, due to the large deflection of the cracked chord, which subsequently caused the diagonal to fail as seen in Figure 8. This failure of the diagonal was secondary to the failure of the chord. This failure mode is different from the static test of the as-is connection in the previous study (Pantelides and Nadauld 2001). In this case, the weld performed well and the base material at the toe of the weld was seen to be the primary failure mode. In the previous study, the failure was through the throat of the weld.

(a)   (b)
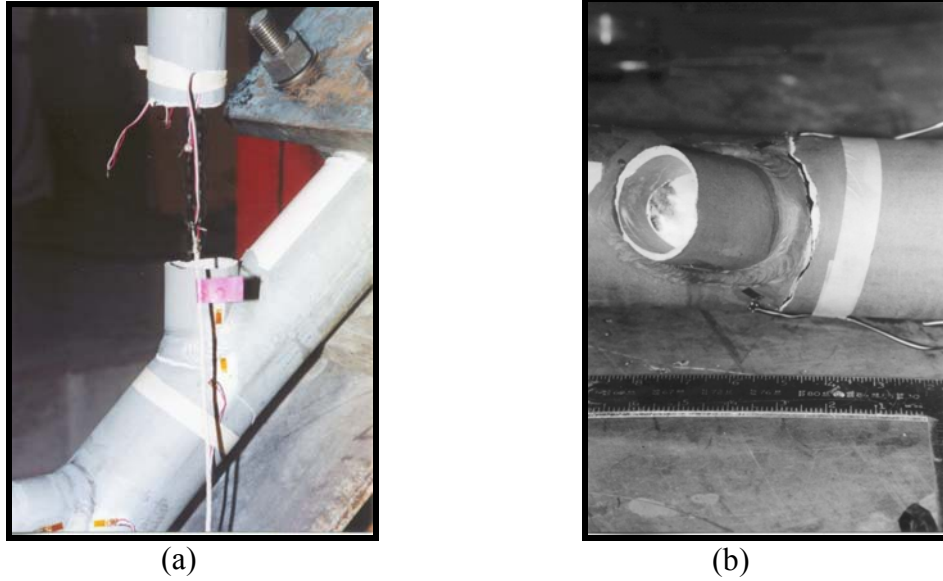
Figure 7. Test I-a: (a) Failure of Diagonal, (b) Failure of chord at toe of weld
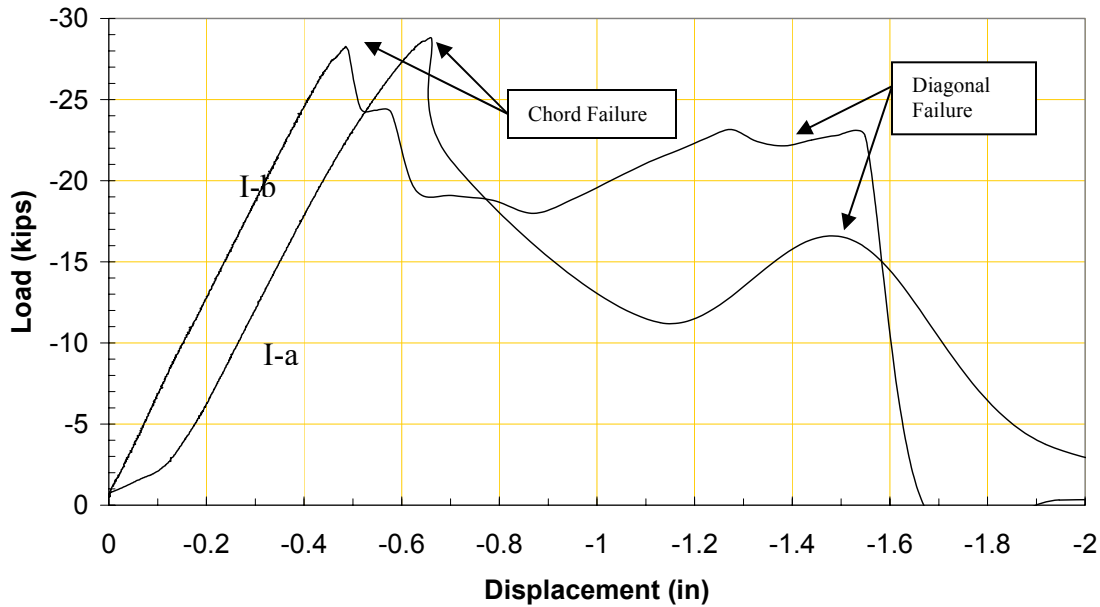
Figure 8. Test I-a and I-b Load vs. Displacement curves

Series (II) Results

Two failure modes were observed in the Series (II) testing: (1) Fracture of the weld through the throat, and (2) crack initiation at the throat of the weld through the base metal, that propagates to the chord. The first failure mode observed was fracture of the weld, through the throat of the weld. This failure was observed in tests II-a (1) and II-d, and is similar to that of static test TS3 of the previous study (Pantelides and Nadauld 2001). In test II-a (1) the failure

was a result of fatigue loading of the test unit, as shown in Table 3. Figure 9(a) shows the crack prior to failure, and Figure 9(b) shows the chord of the failed test unit. The crack shown in Figure 9(a) was first observed to occur at the toe of the weld and propagated from that point, until a rapid failure of the remaining weld occurred.

In test II-d the failure was a result of static loading after being fatigued to 1×10^6 cycles. Prior to the static test there was no visible crack in the weld. The load, displacement, and damage curves for this test are shown in Figures 10(a), (b), and (c), respectively. From Figure 10(a) it can be seen that the maximum load was not constant through the test. This loading sequence was not intended, but was a result of the testing system. This problem was only encountered for the tests that were conducted at a load less than 10 kips. Despite the varying loading, it can be seen that the Cumulative Damage remained relatively constant through the duration of the test. The maximum damage calculated was 0.22, which means the stiffness was reduced by 22% over the 1×10^6 cycles. The failed specimen after the static test is shown in Figures 11(a) and 11(b); the static load–displacement curve for test II-d after 1×10^6 is shown in Figure 11(c).

(a)   (b)
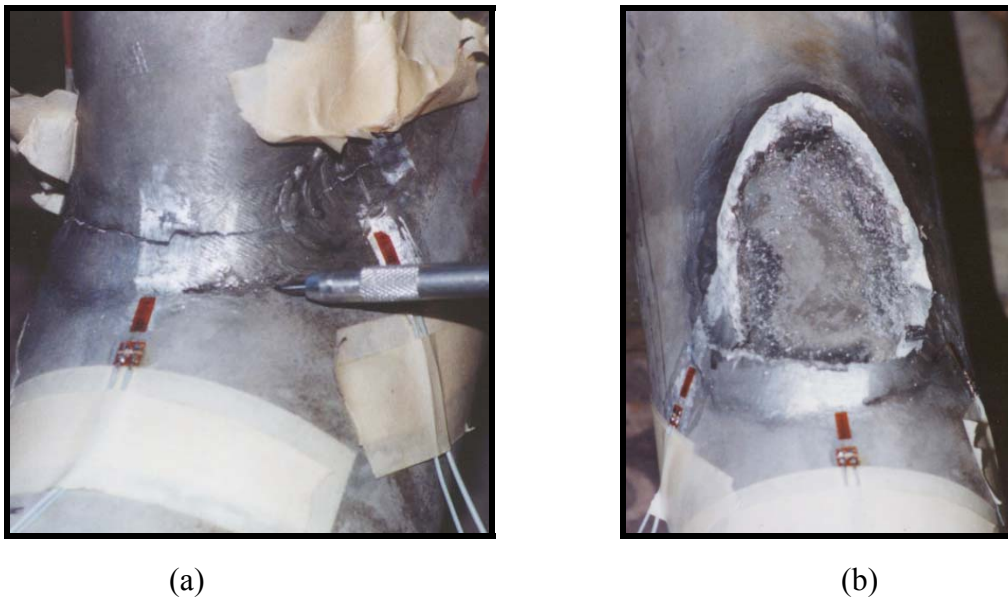
**Figure 9. Test II-a (2): (a) cracking through weld prior to failure, (b) chord after failure**
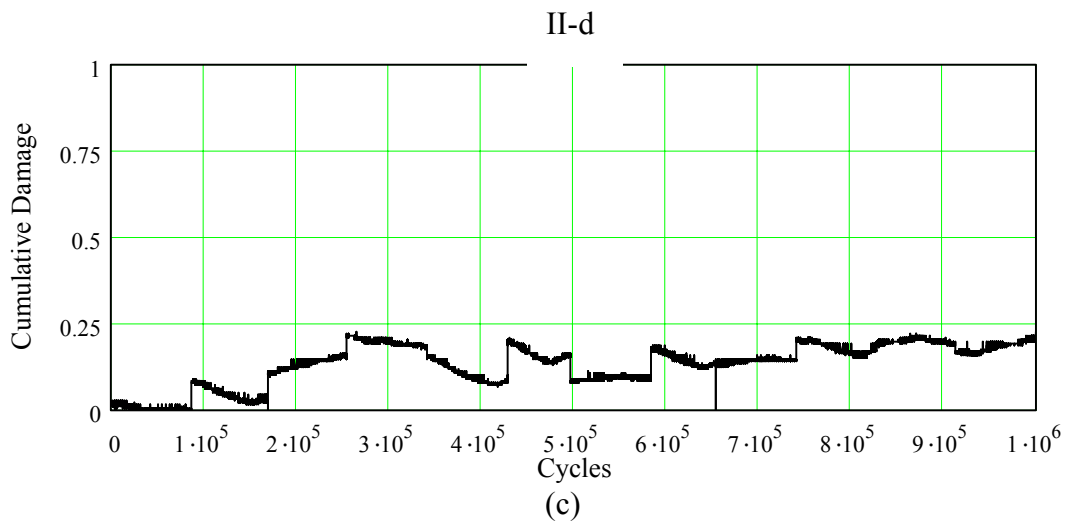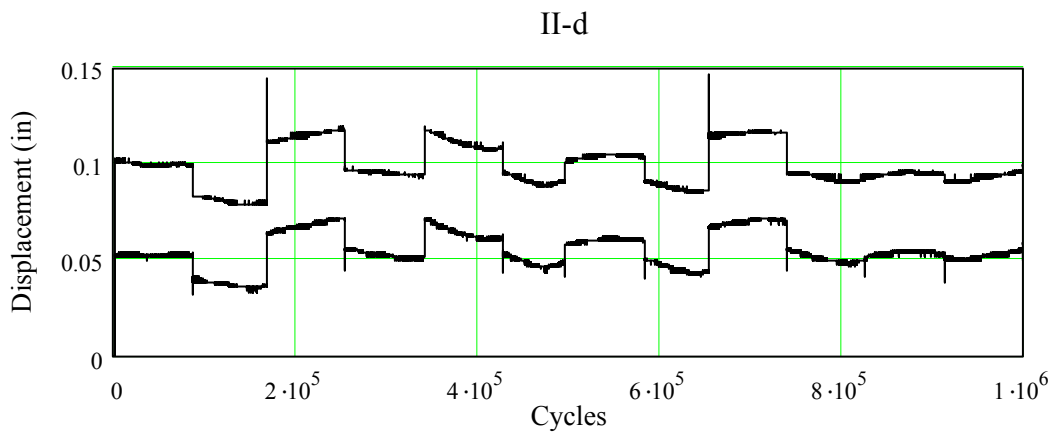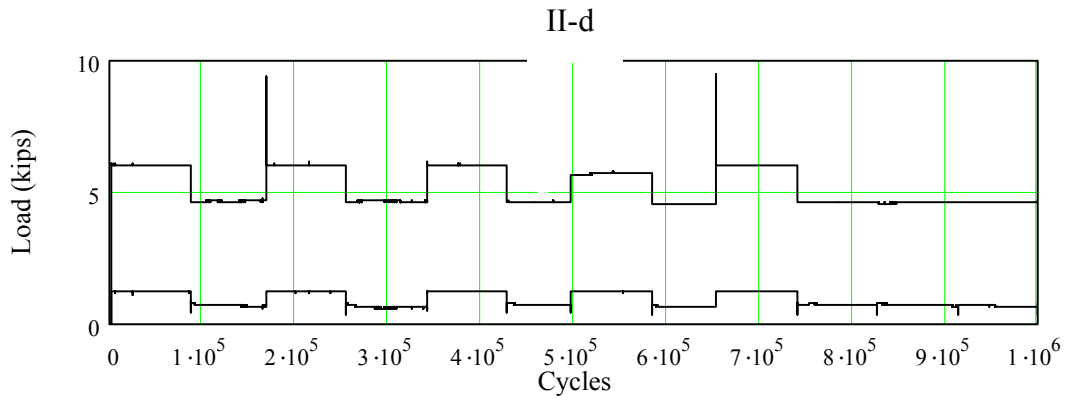
Figure 10. Test II-d: (a) Load – Cycles, (b) Displacement – Cycles, (c) Cumulative Damage – Cycles plots

(a)

(b)

II-d
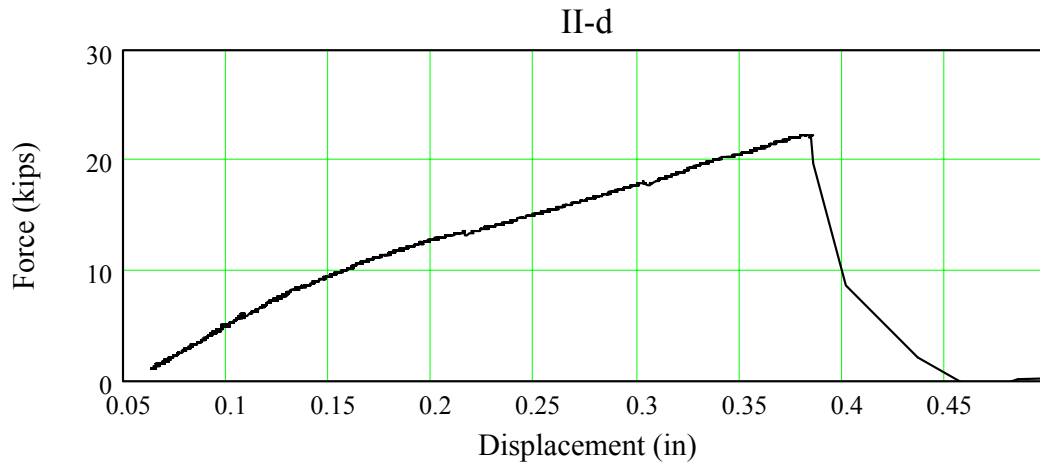
Displacement (in)

(c)

Figure 11. Static Load Test for Specimen of Test II-d after 1x10^6 cycles: (a) diagonal and chord, (b) failure plane on chord, (c) Force–Displacement curve

The second failure mode for the Series (II) testing was observed in tests II-a (2), II-b (1), II-b (2), and II-c. The failure consisted of a crack initiated at the toe of the weld, through the base metal. The crack then propagated away from the weld through the chord, and would have continued around the chord – similar to the failure of the series I tests, as shown in Figure 12(a). However, the steel pipe inside the chord forced the crack to propagate through the base material outside the weld, a distance of ½" to 1" following the weld contour, as shown in Figure 12(b). Figures 13, 14, 15, and 16 show the load, displacement, and cumulative damage curves for tests II-a (2), II-b (1), II-b (2), and II-c, respectively. In all of the fatigue plots failure is indicated by

N_f, which is the number of cycles to failure. All four tests follow the same pattern of damage, with the onset of cracking represented by the increase of slope in the cumulative damage curves. This was verified by test observations. For example, in test II-a (2) the first visible crack appeared at 12,000 cycles. As can be seen in Figure 13, at 12,000 cycles the cumulative damage begins to increase – showing the presence of a crack. The damage immediately before complete failure of the joint varied from 0.45 to 0.79. For all of the tests the damage was less than 0.25 for the majority of the test, demonstrating that most of the damage occurs in the last 20 to 30 percent of the total fatigue life of the joint.

(a)	(b)

Figure 12. Fatigue test of as-is welded joint Test II-b: (a) crack prior to failure, (b) Typical failure of Series II tests
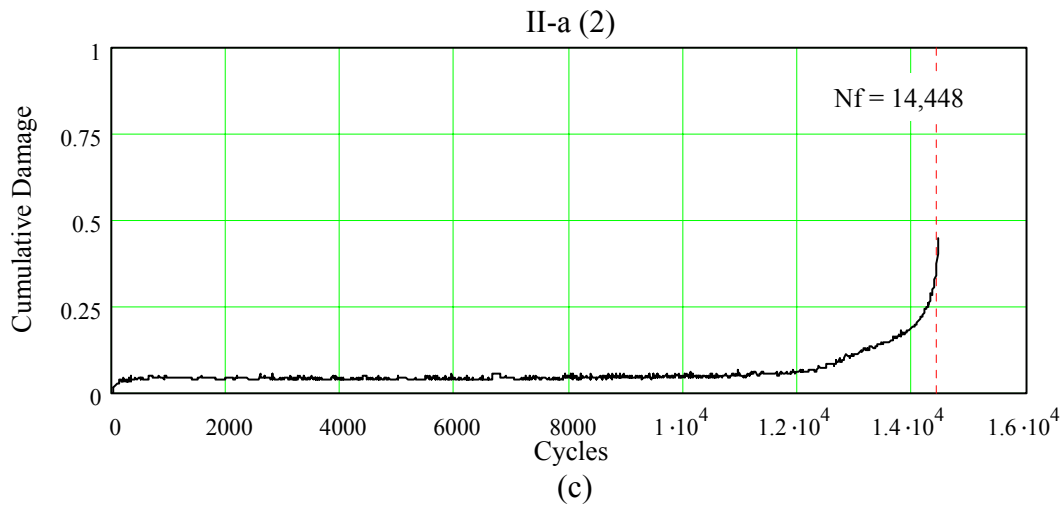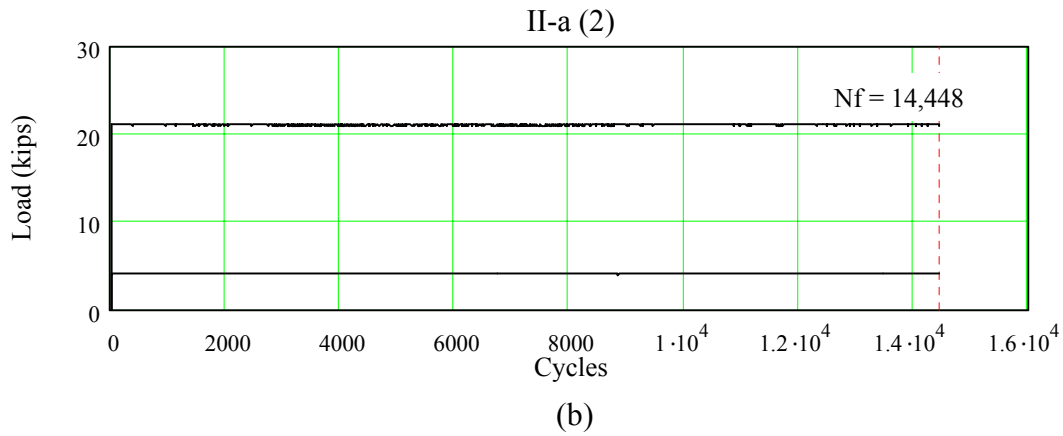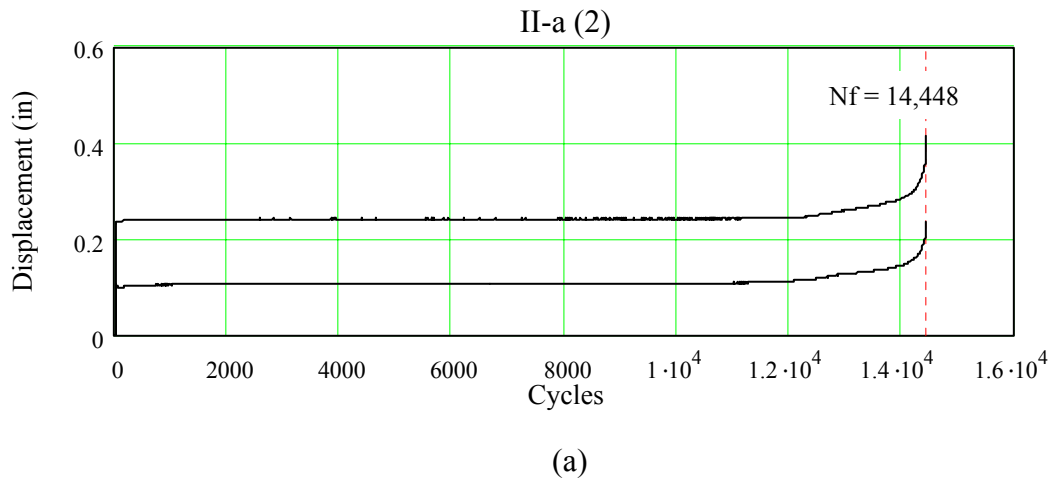
Figure 13. Test II-a (2): (a) Load – Cycles, (b) Displacement – Cycles, (c) Cumulative Damage – Cycles plots
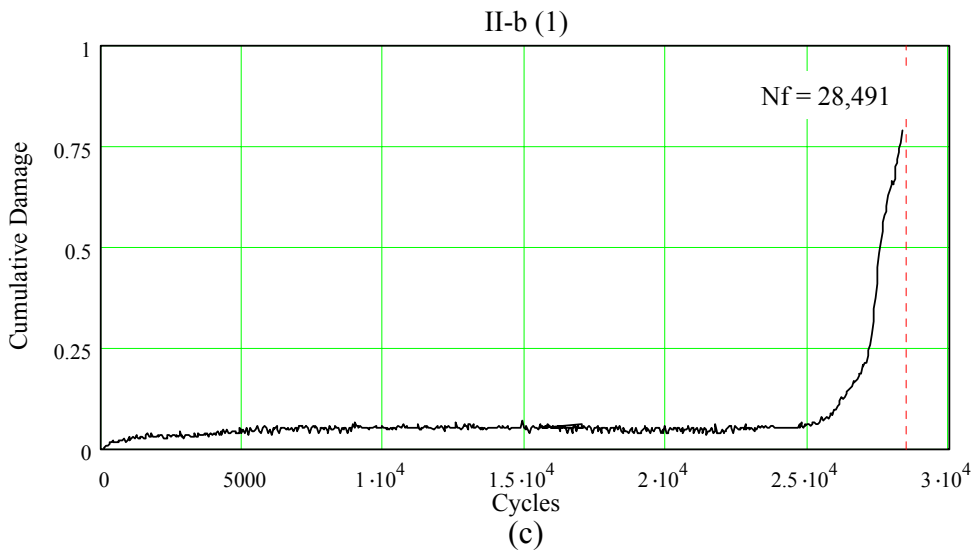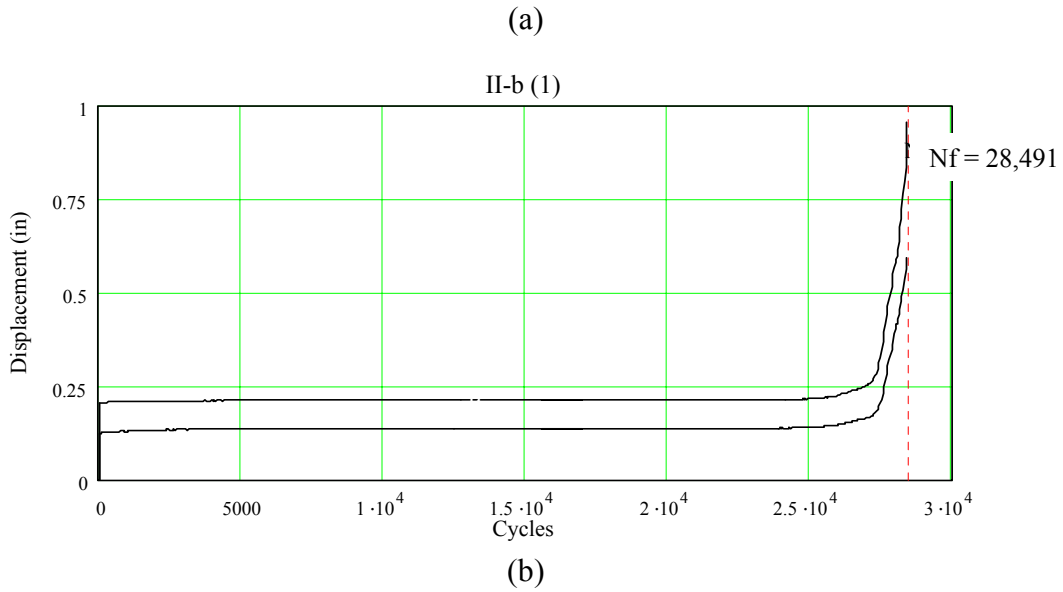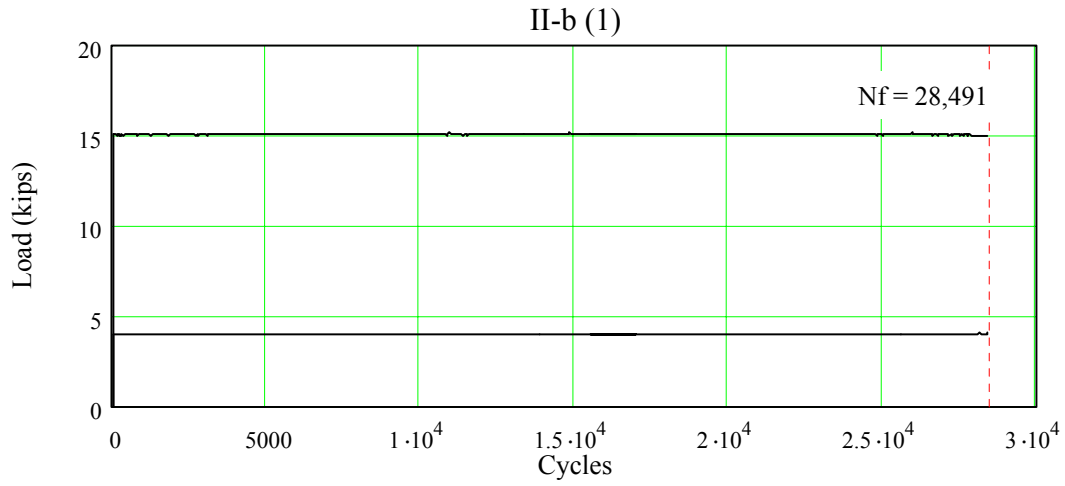
**Figure 14. Test II-b (1): (a) Load – Cycles, (b) Displacement – Cycles, (c) Cumulative Damage – Cycles plots**
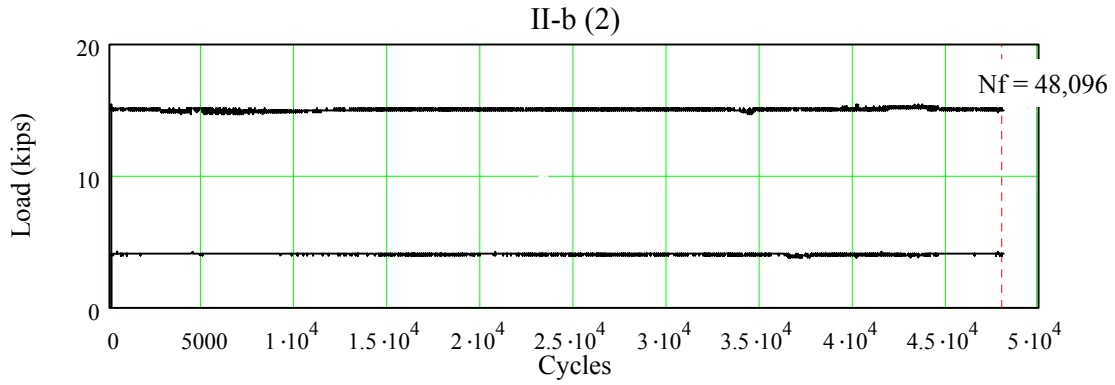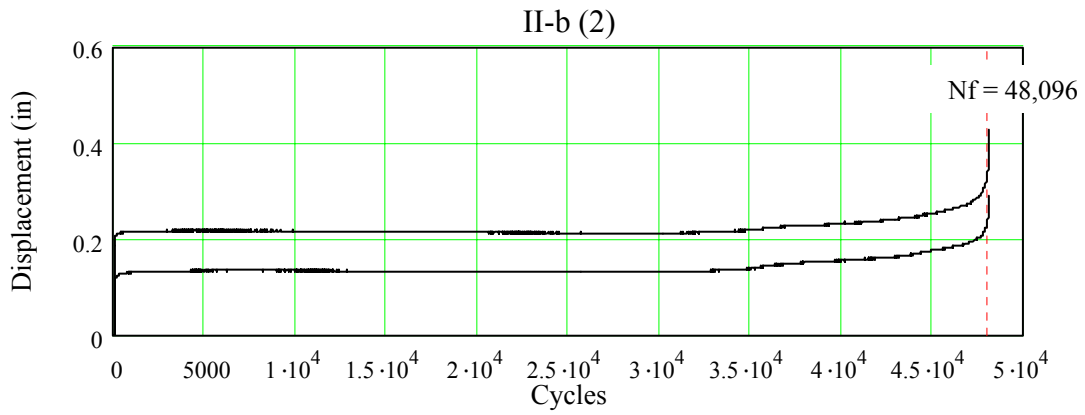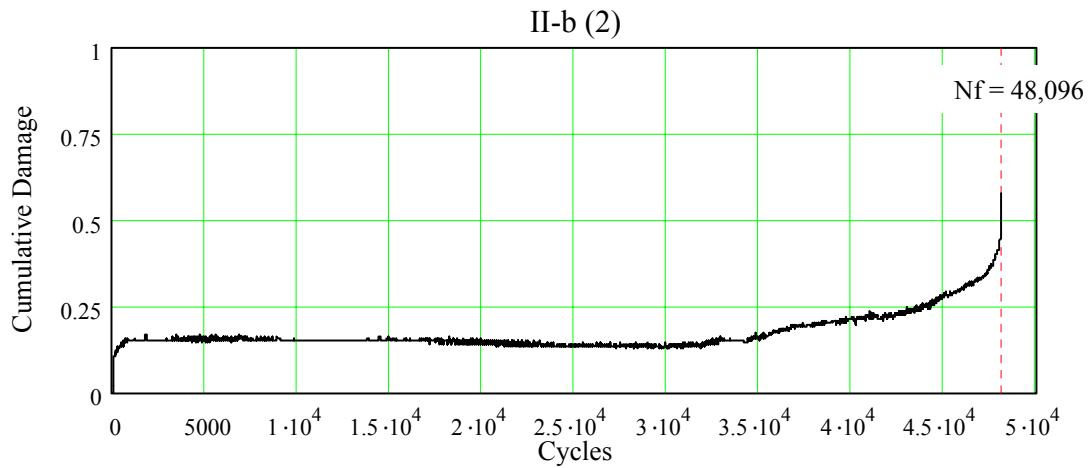
Figure 15. Test II-b (2): (a) Load – Cycles, (b) Displacement – Cycles, (c) Cumulative Damage – Cycles plots
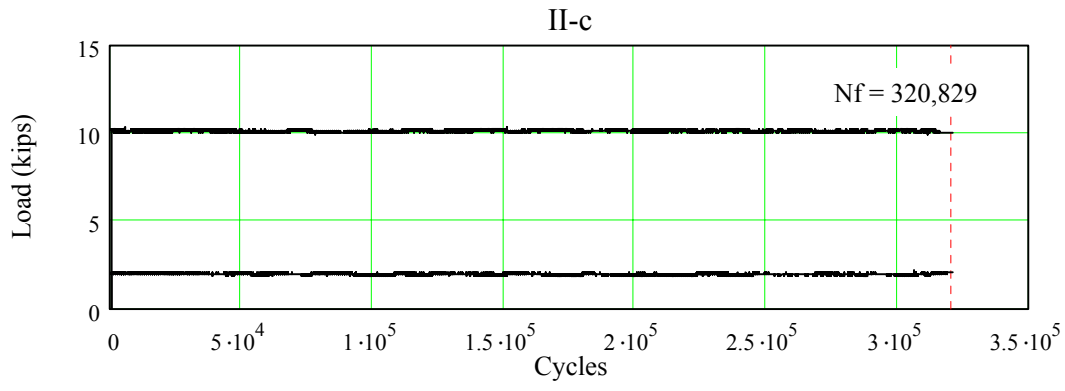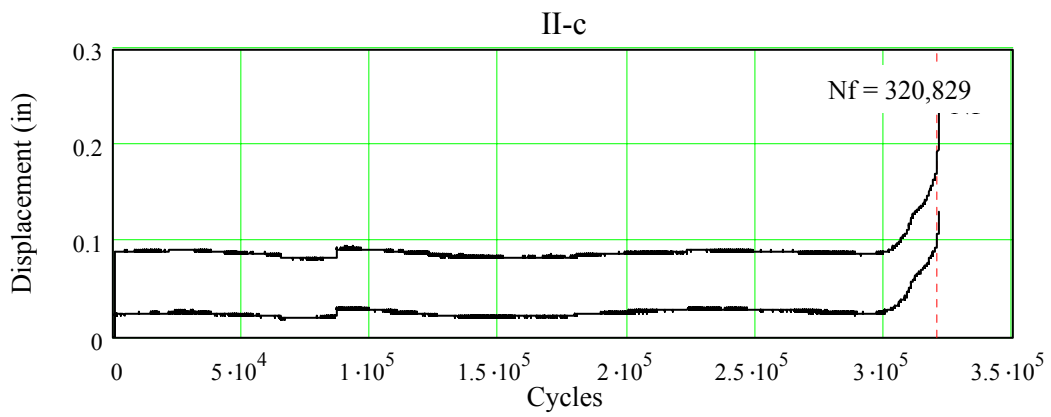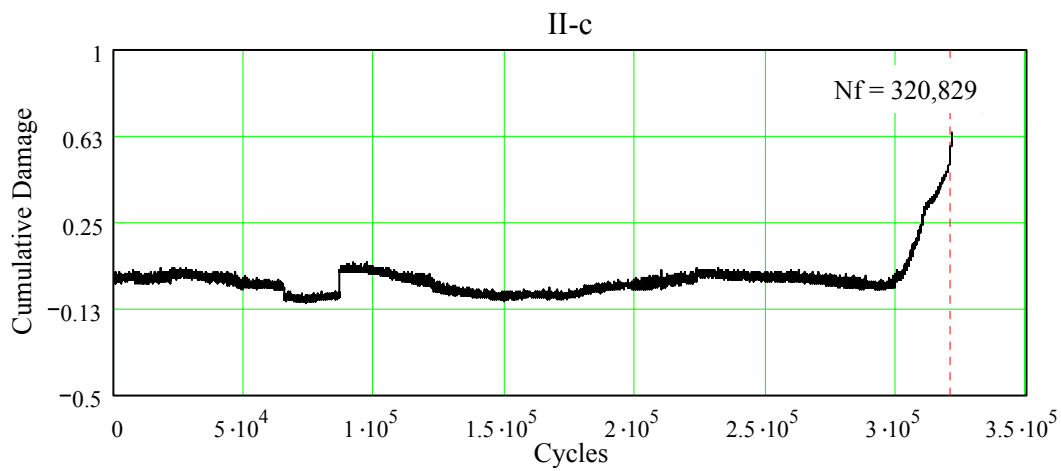
Figure 16. Test II-b (2): (a) Load – Cycles, (b) Displacement – Cycles, (c) Cumulative Damage – Cycles plots

23

Series (III) Results

Failure Mode 1: Weld Throat Cracking and FRP Tensile Failure

Series (III) tests had two basic failure modes: (1) cracking through the throat of the weld and FRP tensile failure, and (2) cracking through the toe of the weld, followed by cracking through the throat of the weld and FRP tensile failure. The first failure mode occurred in tests III-a and III-d and is shown in Figure 17 and Figure 18. This failure consisted of initial cracking of the FRP composite (note the horizontal lines in Figure 17) followed by cracking failure through the throat of the weld and finally by tensile failure of the FRP composite. The load, displacement, and cumulative damage curves are shown in Figure 19 for test III-a, and Figure 20 for test III-d. It can be seen in Figure 19(b) and (c) that the weld failed at about 5000 cycles, and the FRP failed much later at 6763 cycles. From Figure 19(c) it is also evident that the damage did not increase as rapidly near the failure point, as compared to the Series (II) tests. This indicates that for this particular failure mode, the failure is more brittle than that of the Series (II) tests. This is also shown by the lower cumulative damage of 0.33 at failure for test III-a, which is slightly less than the comparable test II-a (2).

Test III-d lasted the pre-determined infinite-life-limit of $1x10^6$ cycles, and was subsequently tested in static tension to failure, as shown in Figure 18. Of all the tests in the present research and the previous research (Pantelides and Nadauld 2001), test III-d obtained the largest static tensile load of 44.17 kips at a displacement of 0.75 in., as shown in Figure 21. This test also had the least damage after reaching $1x10^6$ cycles; the maximum cumulative damage was 0.19, as shown in Figure 20(c). The cause of this large static strength and superior fatigue behavior is not clear.

(a)   (b)
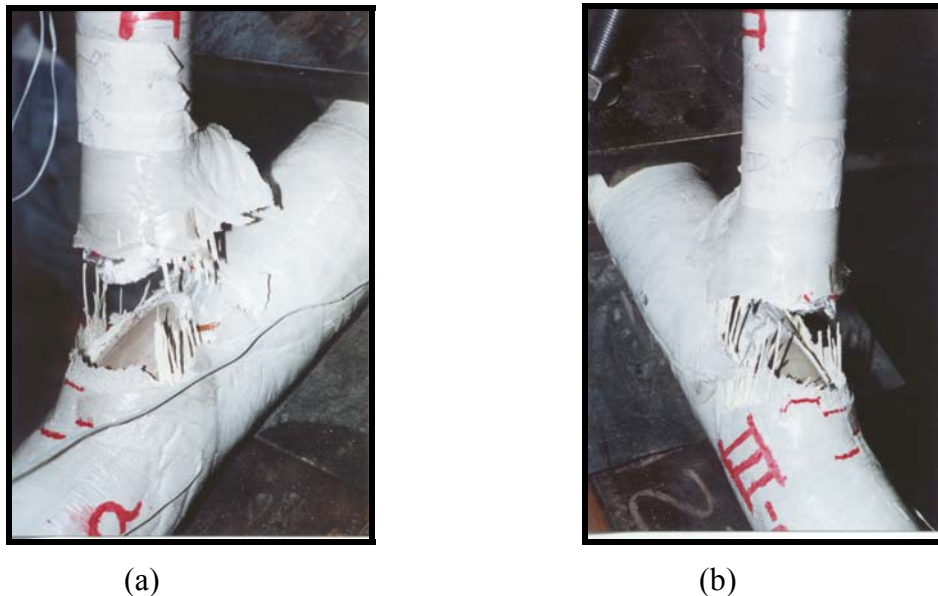
Figure 17. Test III-a: (a), and (b) Failure of weld and FRP composite

| (a) | (b) | (c) |

Figure 18. Test III-d: (a), (b), and (c) Failure of weld and FRP composite

III-a

(a)

III-a

(b)
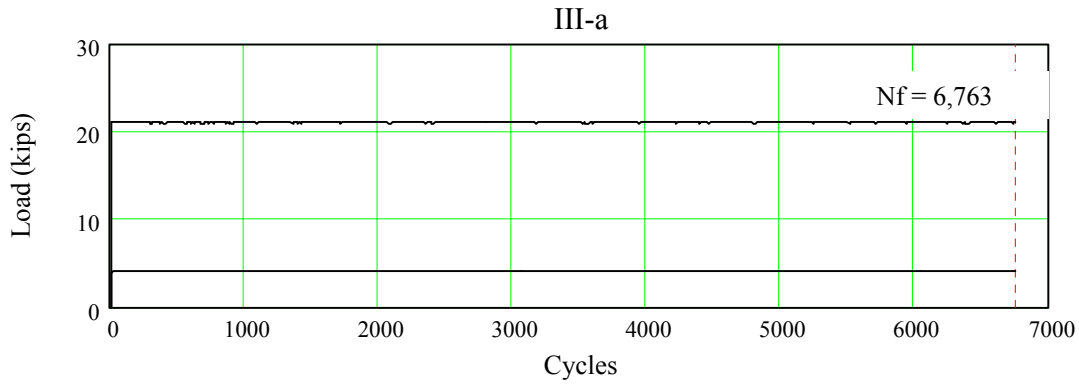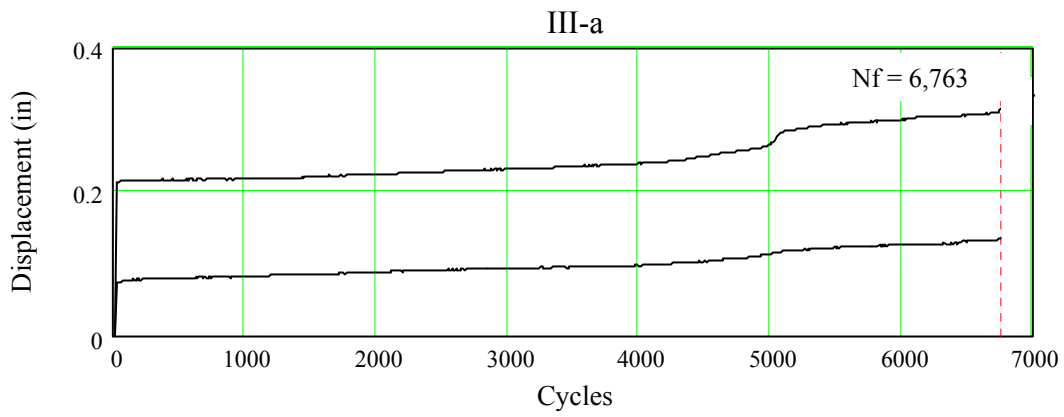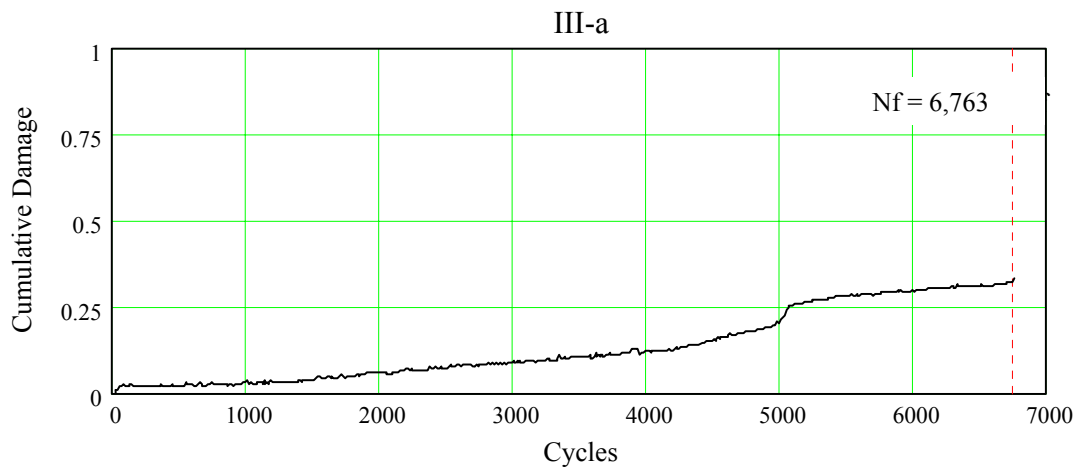
III-a

(c)

Figure 19. Test III-a: (a) Load – Cycles, (b) Displacement – Cycles, (c) Cumulative Damage – Cycles plots
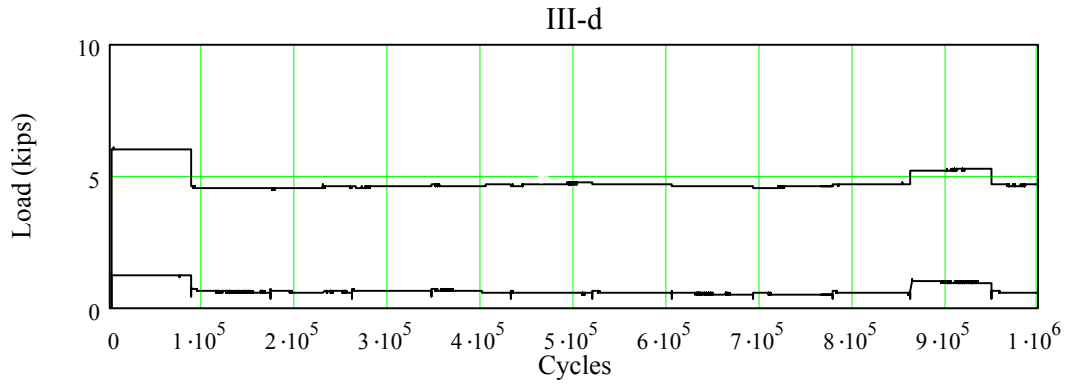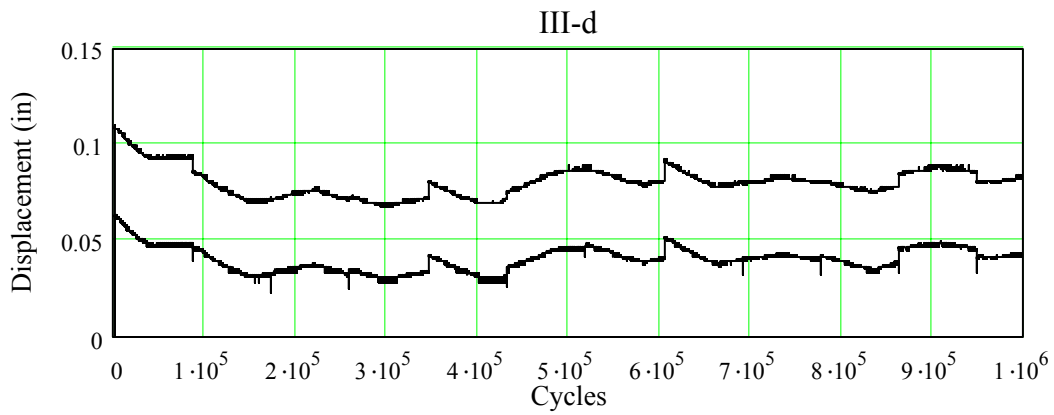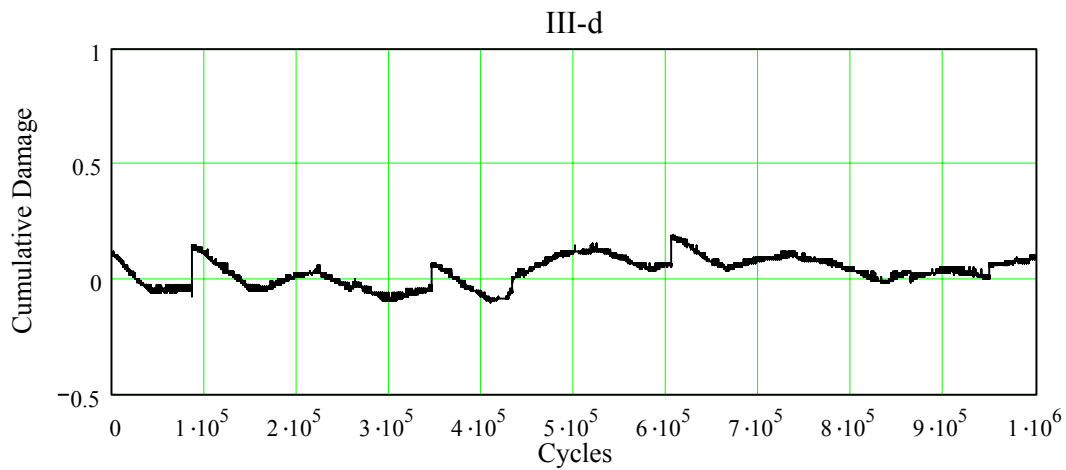
**Figure 20. Test III-d: (a) Load – Cycles, (b) Displacement – Cycles,
(c) Cumulative Damage – Cycles plots**
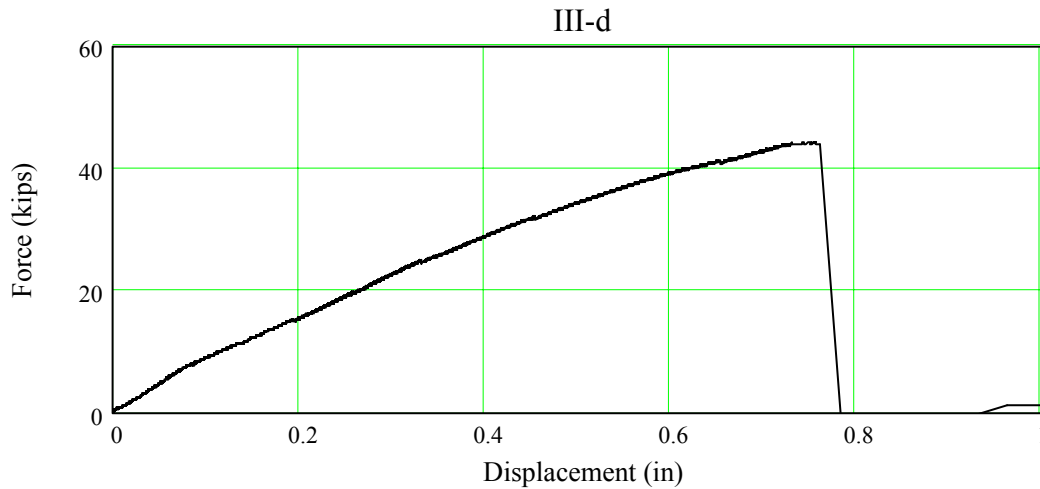
Figure 21. Test III-d: Static Load – Displacement curve after $1x10^6$ cycles

Failure Mode 2: Toe Weld Cracking followed by Throat Weld Cracking and FRP Failure

The second failure mode seen in the Series (III) tests is shown in Figures 22 and 23. This failure was seen in tests III-b and III-c. In this failure mode, cracking was seen in the FRP first. This cracking was directly above the initial crack of the aluminum at the toe of the weld; this failure was not through the throat of the weld. This crack at the toe of the weld propagated around the chord, similar to the failure mode of Series (II) tests. Next the weld was slowly fatigued; this occurred in the throat of the weld, until the weld completely fractured. This was followed by tensile failure of the FRP composite.

In test III-b these stages of failure can be seen in Figures 24(b) and (c). Between 8,000 and 12,000 cycles there is a lot of damage occurring until the cumulative damage reaches 0.50. This large amount of damage is caused by the initial crack at the toe of the weld. At this point the damage slowly increased until it reached 0.57, at 67,300 cycles. This damage is caused mostly by continued crack growth at the toe of the weld, fatigue through the remaining throat of the weld, and fatigue of the FRP composite. Finally, the last stage shows the damage increasing from 0.57 to 0.79 immediately prior to complete failure of the joint. This damage and ultimate failure shows the complete failure of the remaining weld and rupture of the FRP composite. It is important to note that the weld was carrying only a small portion of the load after the Cumulative Damage reached 0.50, i.e. after 12,000 cycles, and that the FRP was carrying the majority of the load.

Test III-c was fatigued until $1x10^6$ cycles were reached. After $1x10^6$ cycles the crack in Figure 23(a) had formed. The remaining strength of the connection after $1x10^6$ cycles was determined with a tensile static test, as in test Series (I). The static test revealed a failure mode similar to test III-b, i.e. Failure Mode 2, which included failure of the aluminum at the toe of the weld, followed by failure of the weld through the throat of the weld, and finally failure of the FRP composite. These failures can be seen in Figures 25 and 26. In this test these failures occurred immediately after one another, with only 0.72 seconds from initial failure to complete failure. The occurrence of three distinct failure phases was also verified through testing

observations and video, where three distinct failure phases could clearly be seen and heard. It can be seen in Figure 27(c) that after the 1,000,000 cycles, the cumulative damage had only reached about 0.36. This shows that despite the initial growth of the crack at the toe of the weld at the very beginning of the fatigue test, as shown in Figures 27(b) and (c), the crack did not propagate as far as the same crack in test III-b. This is clearly a result of the lower stress level, and the ability of the FRP composite to carry the load after the initial crack in the aluminum.

(a)   (b)
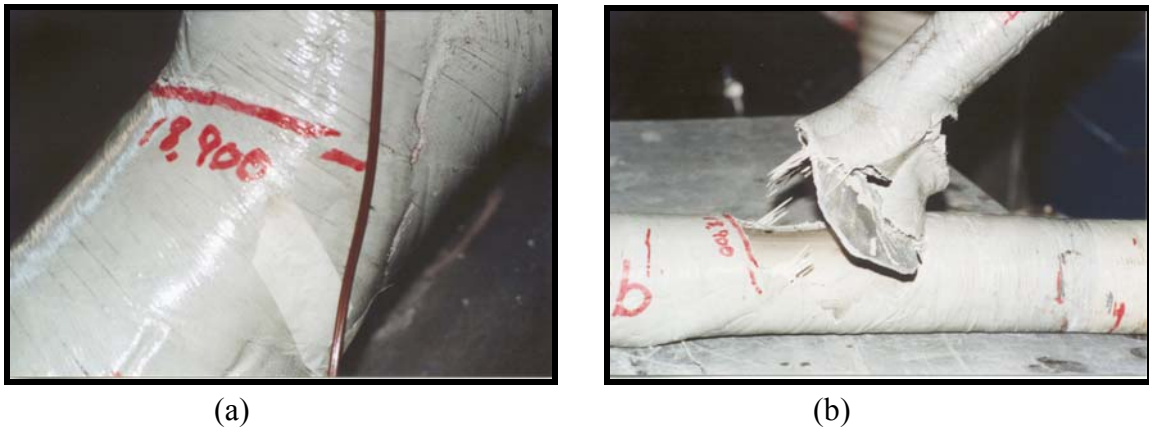
Figure 22. Test III-b: (a) Initial cracking of FRP composite, (b) Failure of Base Material, Weld, and FRP composite

(a)   (b)
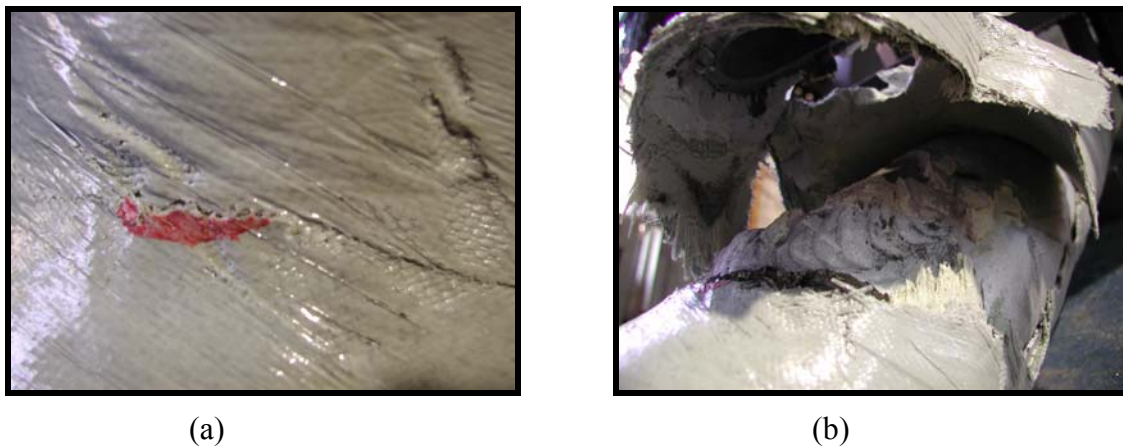
Figure 23. Test III-c: (a) Crack in FRP after 1×10^6 cycles, (b) Picture of III-c after static loading to failure
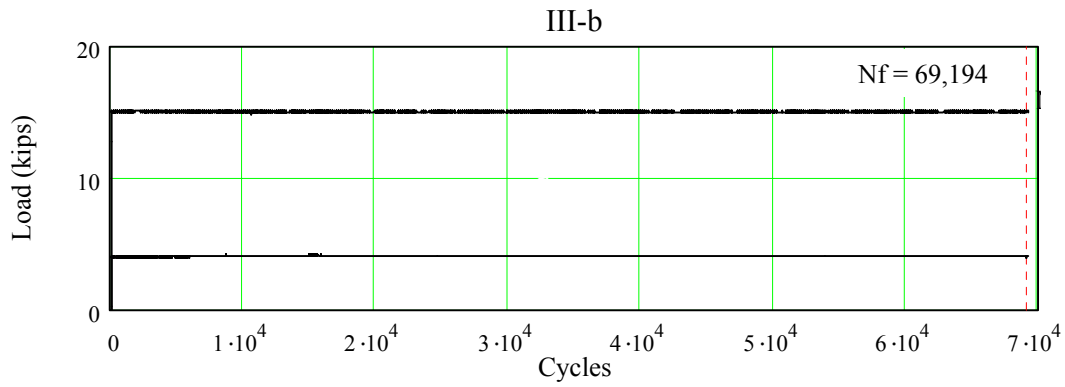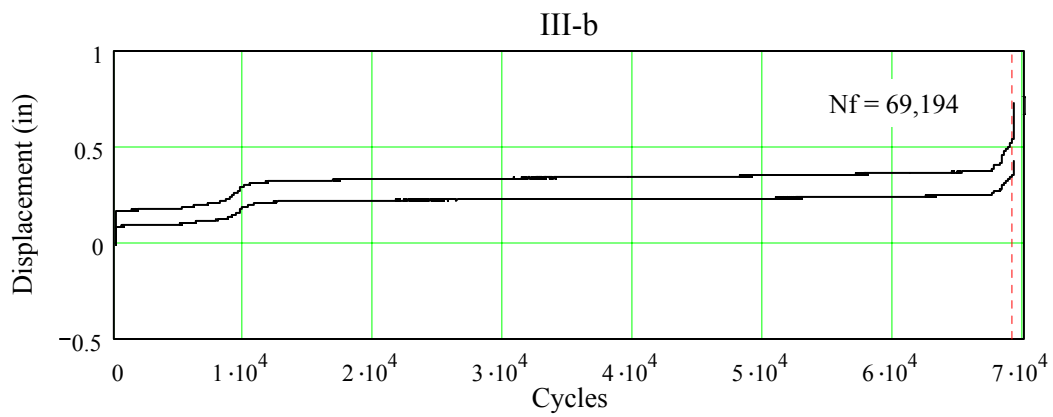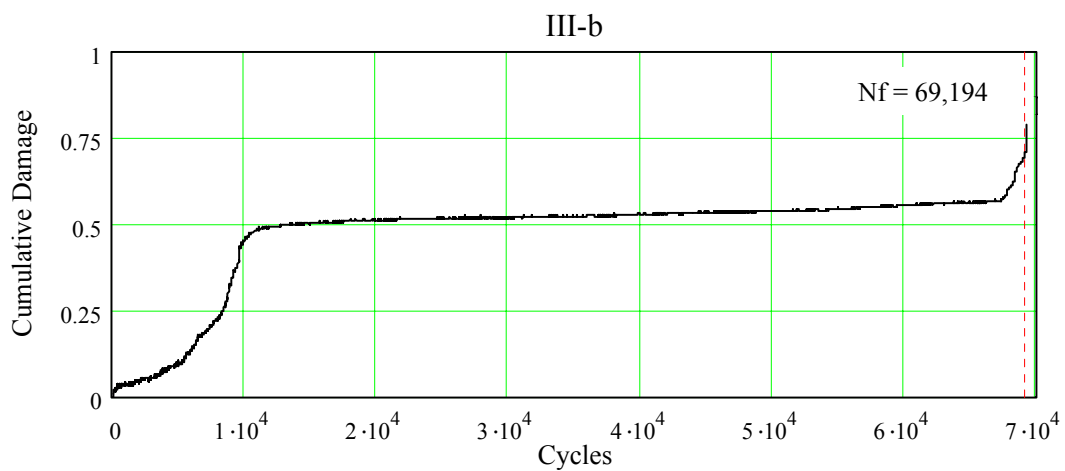
Figure 24. Test III-b: (a) Load – Cycles, (b) Displacement – Cycles,
(c) Cumulative Damage – Cycles plots
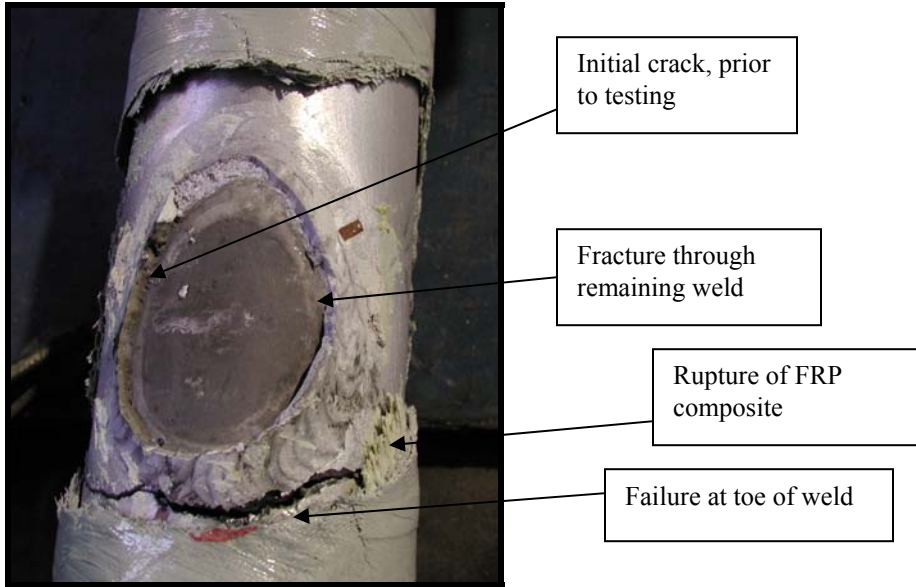
Figure 25. Picture of test III-c after static test showing failure stages
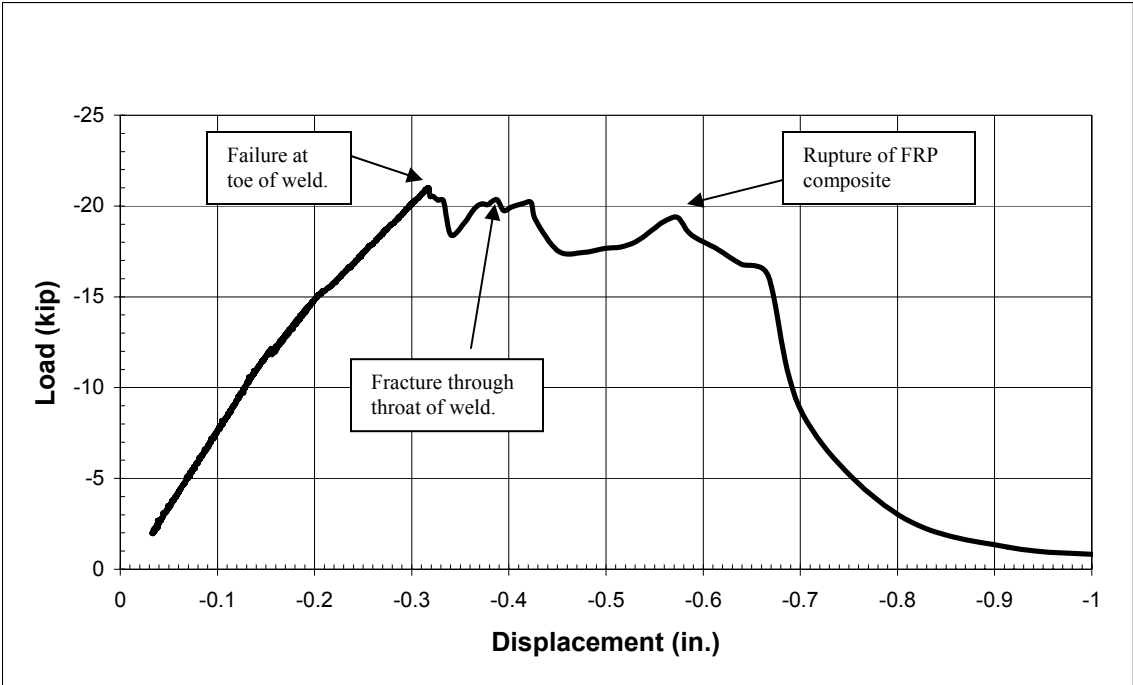
Figure 26. Static test of test III-c after 1x10^6 cycles

III-c

(a) Load – Cycles plot

III-c

(b) Displacement – Cycles plot

III-c

(c) Cumulative Damage – Cycles plot
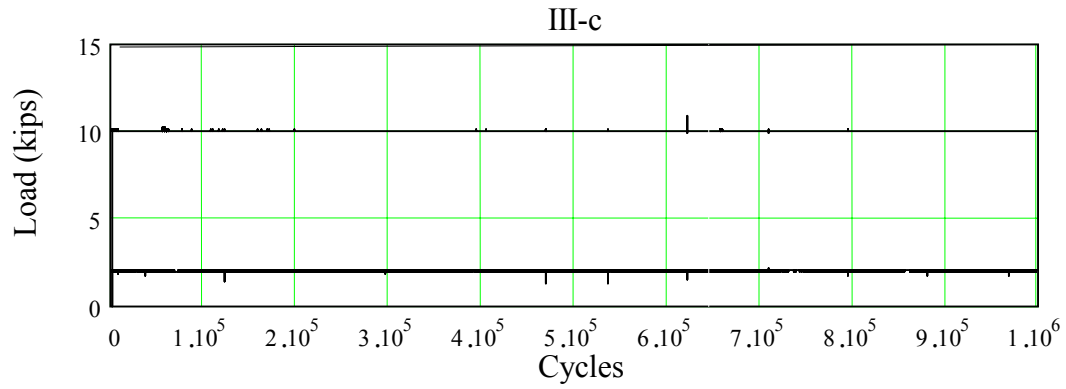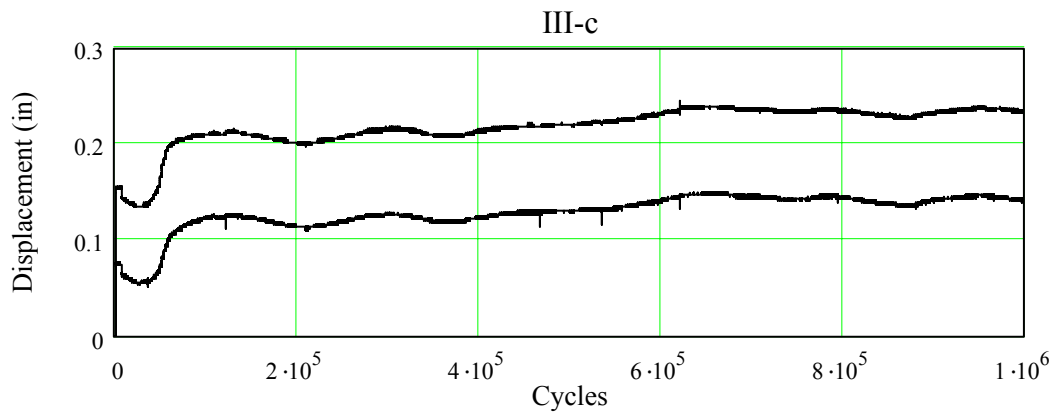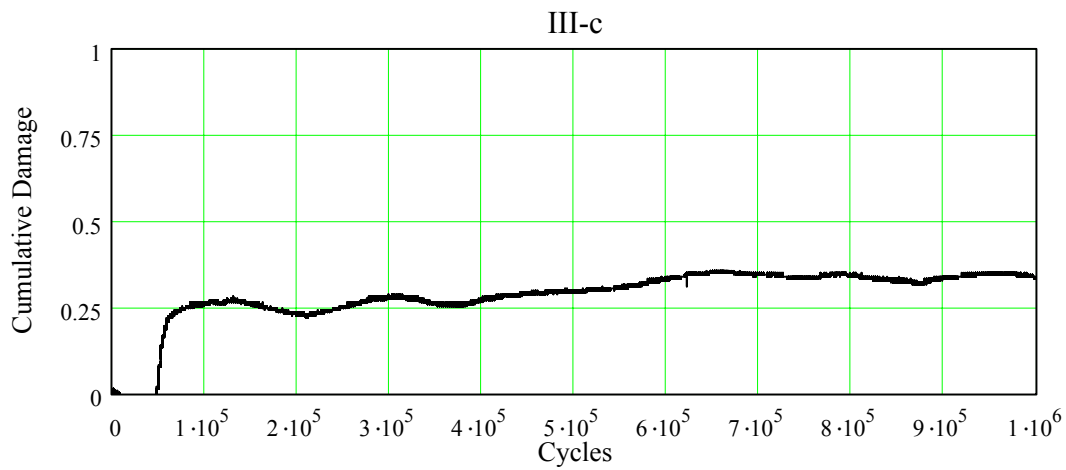
**Figure 27. Test III-c: (a) Load – Cycles, (b) Displacement – Cycles,
(c) Cumulative Damage – Cycles plots**

32

Series (IV) Results

Failure Mode 1: Adhesive Failure

Series (IV) tests had two failure modes: adhesive failure, and FRP composite tensile failure. The adhesive failure occurred in tests IV-a (1) and IV-c. The adhesive failure of tests IV-a (1) and IV-c is shown in Figure 28. This failure is identical to the adhesive failure described in the previous report regarding static tests of similar joints (Pantelides and Nadauld 2001). In this failure mode, the aluminum tube simply pulls out of the FRP jacket. For more information regarding this failure mode consult the previous report (Pantelides and Nadauld 2001). Figures 29 and 30 show the load, displacement, and cumulative damage curves for tests IV-a (1) and IV-c, respectively. Figure 29 shows the load and displacement curves as continuous plots, rather than envelopes of the maximum and minimum values. This was done due to the small number of cycles to failure in this test, and to allow the reader a better understanding of what occurred during the test. It can be seen that test IV-a (1) did not perform very well, and must have been very close to its static tensile capacity. This is shown by the low amount of cumulative damage prior to failure, which was only 0.20 as compared to 0.33 in test III-a. This indicated that the failure was rather abrupt, and would give very little warning as to impending failure. This same behavior was observed in test IV-c, as shown in Figure 30. The cumulative damage was only 0.24 just prior to failure, which indicates even less warning as to impending failure.

(a)   (b)
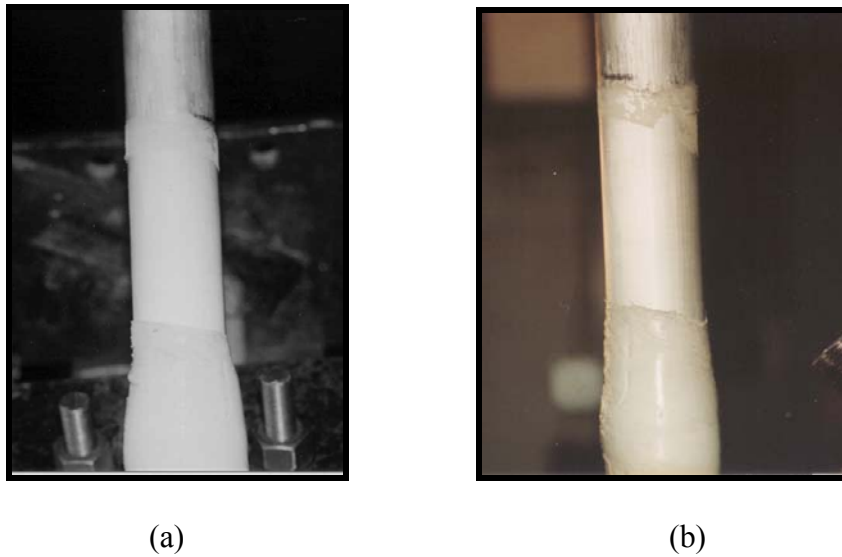
Figure 28. Adhesive failure (a) IV-a (1), (b) IV-c
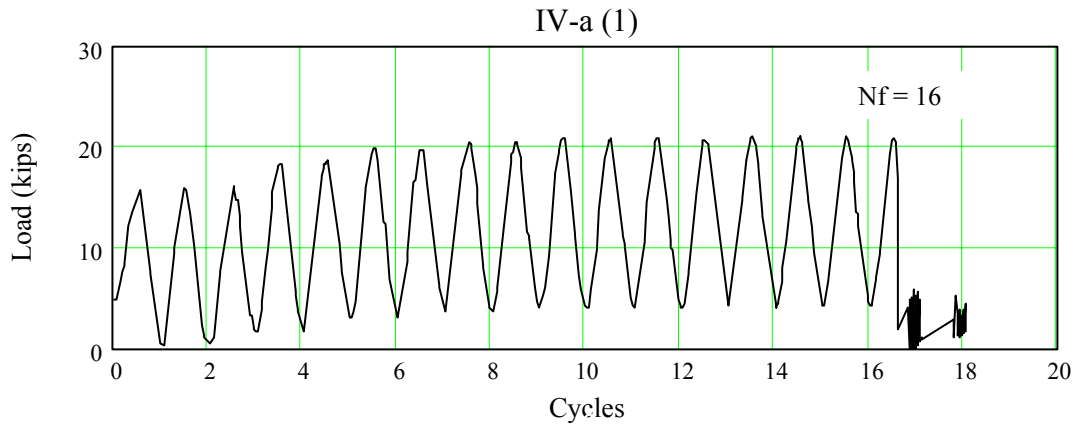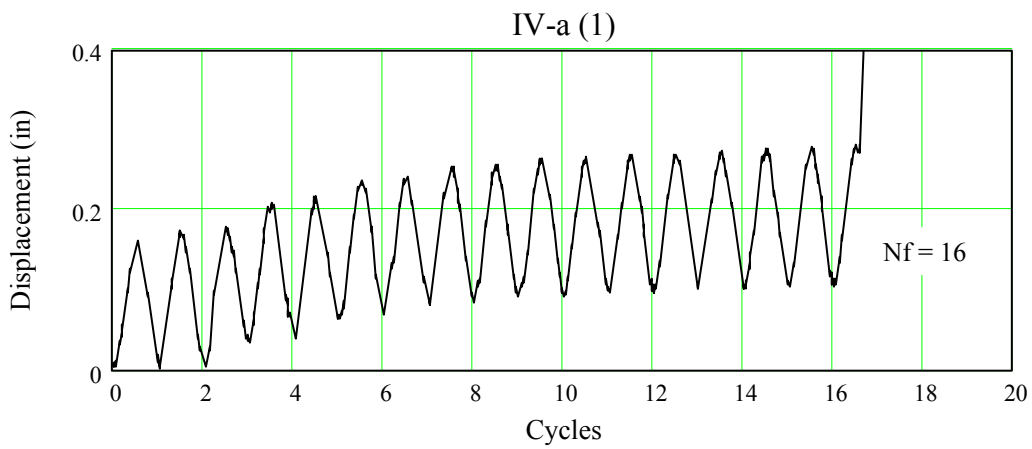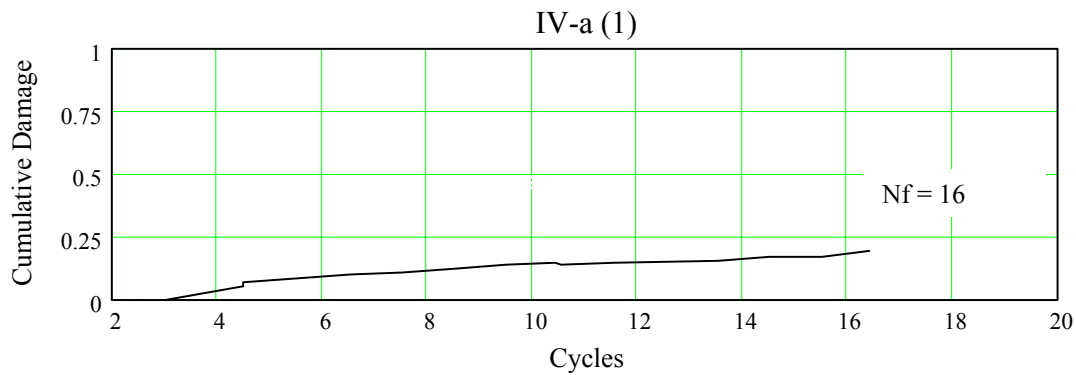
Figure 29. Test IV-a (1): (a) Load vs. Cycles, (b) Displacement vs. Cycles, (c) Cumulative Damage vs. Cycles
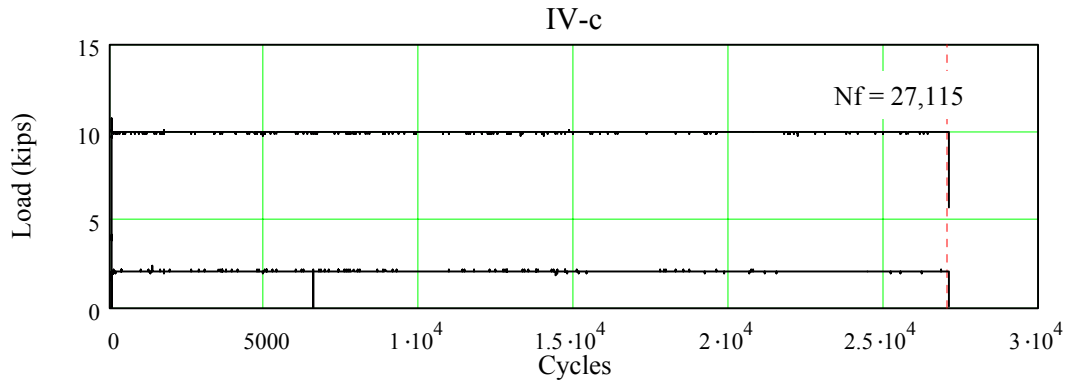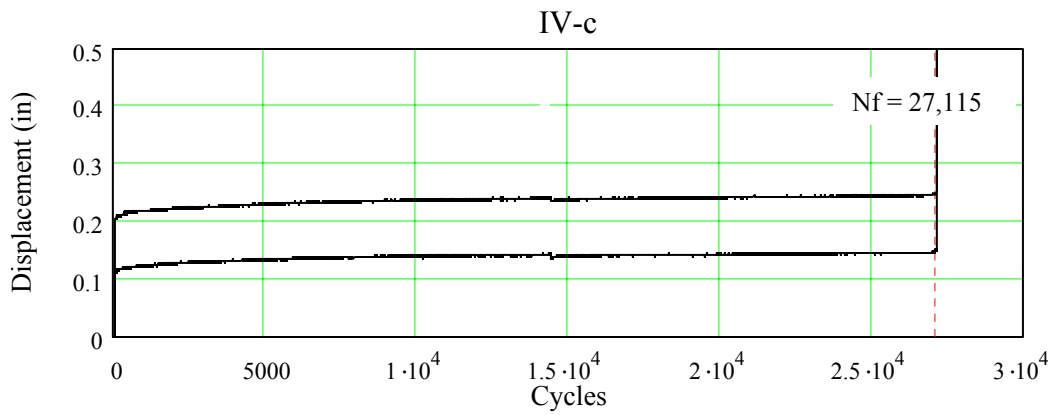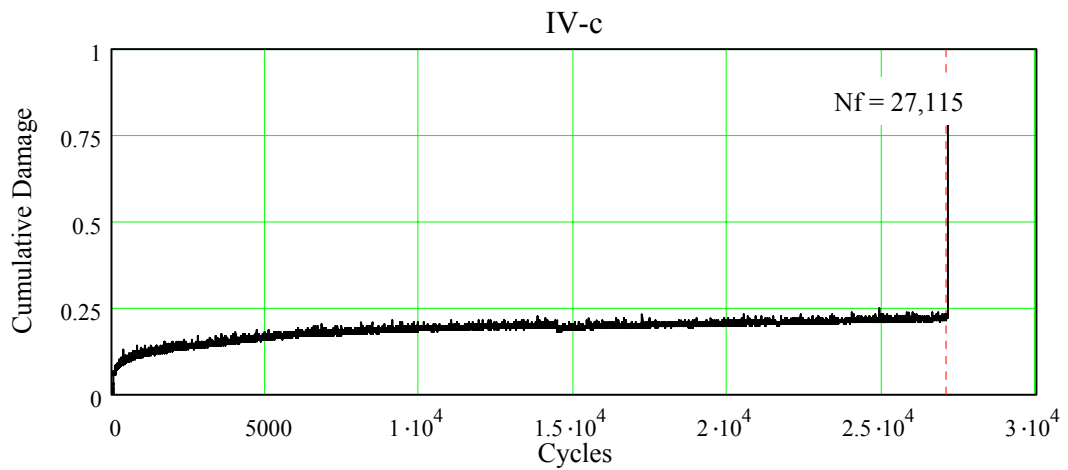
Figure. 30. Test IV-c: (a) Load vs. Cycles, (b) Displacement vs. Cycles, (c) Cumulative Damage vs. Cycles

35

Failure Mode 2: FRP Composite Tensile Failure

Failure mode 2 is the tensile failure of the FRP composite. Test IV-a was repeated to determine if the adhesive failure was due to quality control issues, during the application of the FRP. This second test, IV-a (2), had an FRP composite tensile failure even though the test unit and loading program were identical to test IV-a (1), as shown in Figure 31. The maximum strain in the GFRP composite for test IV-a (1) was 0.55%, whereas the maximum measured strain for test IV-a (2) was 1.55%. This indicates that there were likely some quality control issues in the preparation of test unit IV-a (1). However, the test results presented in this research are not sufficient to determine definitively the cause of such poor performance for test IV-a (1). For the present investigation it is sufficient to say that test IV-a (1) had lower bond strength than test IV-a (2), which was prepared using the same process and materials. However, both test IV-a (1) and IV-a (2) overall did not perform as well as expected. Figure 33 shows the load, displacement, and cumulative damage curves for test IV-a (2). The load and displacement curves are similar to test IV-a (1), however the cumulative damage curve shows that test IV-a (2) had a much higher cumulative damage, 0.42, just prior to failure. Even though most of the damage occurred in the last few cycles, this result is better than that obtained in test IV-a (1) as it gives more warning of impending failure.

Test IV-b also had an FRP composite failure, as shown in Figure 32. This test also did not perform as well as expected, considering it failed after just 913 cycles. This poor performance is also indicated in Figure 34. It can be seen that the failure occurred suddenly, with very little sign of damage (which was 0.33 just prior to failure), or increased displacement as was seen in the Series (II) and Series (III) tests.

After completion of the above tests it was determined that the poor overall performance of the Series (IV) tests was due to poor bond between the aluminum and the FRP. There may be many reasons for this poor bond. Any aluminum surface exposed to air develops a thin oxide film, which is hard, chemically stable, and tightly keyed to the metal. Though very thin, typical thickness 0.0002 in., this layer prevents further oxidation (Dwight 1999). When damaged, it immediately reforms, provided oxygen is available, and it is this that gives aluminum its good durability. In moderate industrial environments, the aluminum surface will darken and roughen. As the atmosphere becomes more aggressive, the discoloration and roughening increases with visible white powdery oxides. When surface attack occurs, there is a rapid initial loss of reflectivity over 6 to 36 months, thereafter slowing down with little change over the next 10 to 80 years (Bull 1994). Practically all the units from the field had obvious discoloration and roughening, and for some the white powdery oxides were visible.

Because the Series (IV) test units were constructed of new aluminum pipes, which were brand new and not exposed to the atmosphere, the dark and roughened surface observed in the field units was not there; on the contrary, the Series (IV) units had a very shiny and smooth surface. In addition, the aluminum surface of the Series (IV) units contained oils and other elements that were not completely removed in the preparation steps outlined in the first report (Pantelides and Nadauld 2001). Therefore, the poor performance of the Series (IV) units can be attributed to the reduced roughening of the surface and the presence of oils, both of which contributed to the poor bond. In order to determine if the use of new aluminum was having an effect on the performance of the Series (IV) tests, the Series (V) tests were performed.

<div align="center">

(a)   (b)

Figure 31. FRP composite failure of test IV-a (2)

</div>

<div align="center">

(a)   (b)   (c)

</div>

Figure 32. Sequence of failure for test IV-b: (a) 0.004 sec. prior to failure, (b) 0.467 sec. after failure, (c) 1.746 sec. after failure
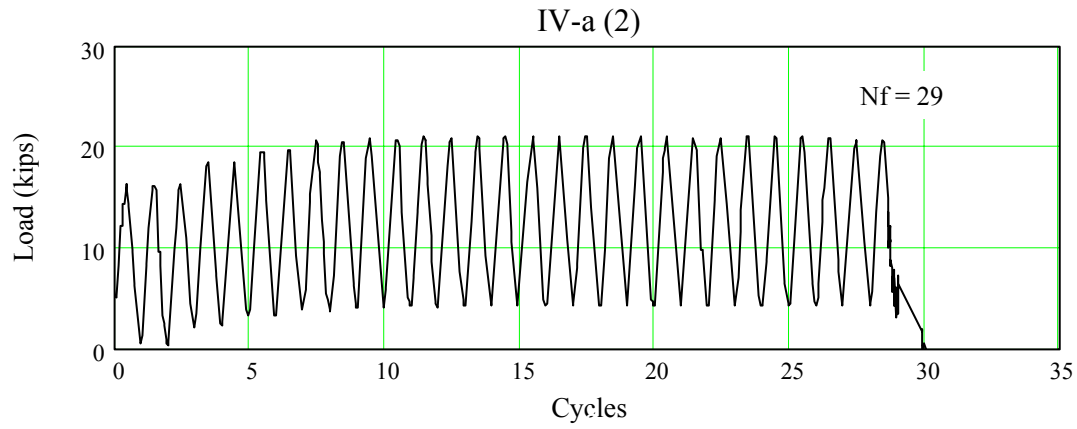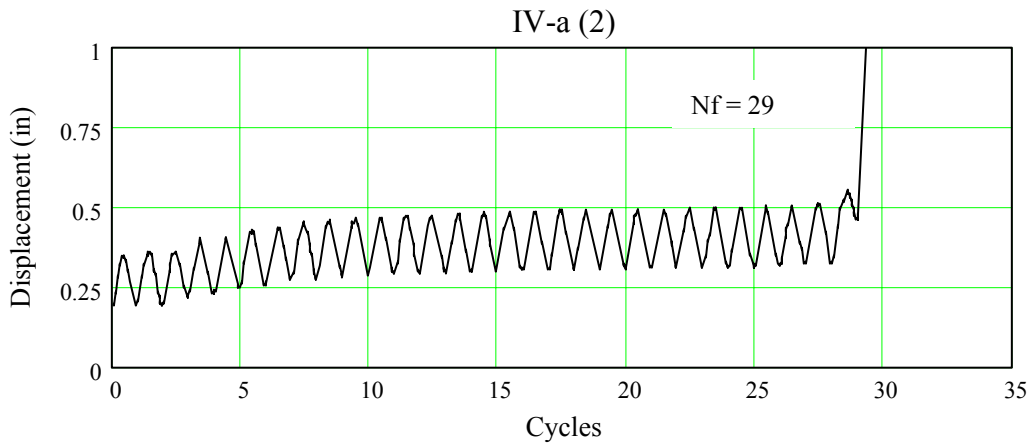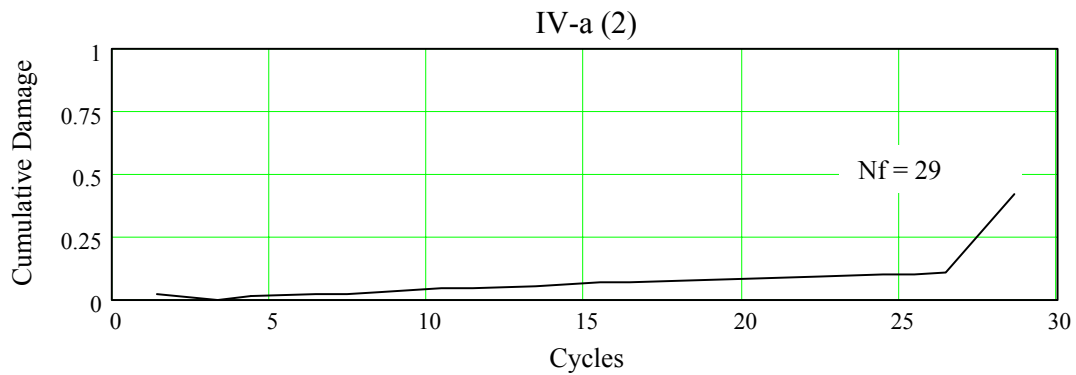
Figure 33. Test IV-a (2): (a) Load vs. Cycles, (b) Displacement vs. Cycles, (c) Cumulative Damage vs. Cycles
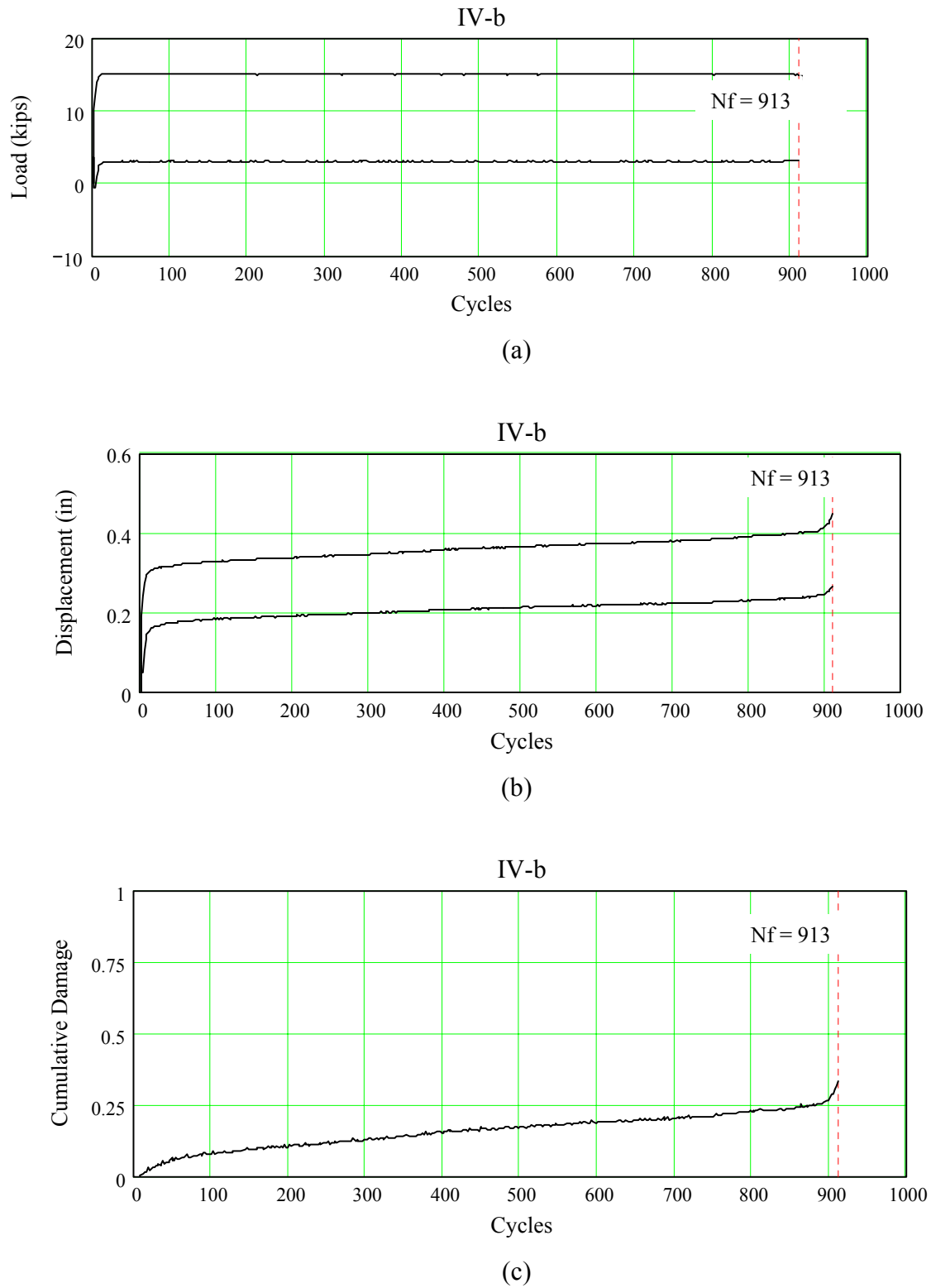
Figure 34.   Test IV-b: (a) Load vs. Cycles, (b) Displacement vs. Cycles, (c) Cumulative Damage vs. Cycles

Series (V) Results

Failure Mode 1: Adhesive with FRP Tearing

This failure mode was only observed in test V-b (1), as shown in Figure 35(a). This type of failure was caused by the decreased bond length of test unit V-b (1) that was about 2 inches shorter than all the other retrofitted test units in this study. However, in this particular test the FRP was also observed to tear open as the aluminum tube was pulled out of the FRP jacket, as shown in Figure 35(a) and (b). This tearing was caused by the weld that remained at the end of the diagonal member, which caused the diameter of the diagonal at the weld to be larger than the pipe diameter. This is certainly an advantage, due to the mechanical interlocking of the diagonal and the FRP, even though this failure mode is the least desirable due to its lower strength and sudden failure. It can be seen in Figure 36 that the cumulative damage of test unit V-b (1) increased very rapidly at the beginning of the test, likely due to the failure of the remaining 10% of the weld. The damage then slowly increased until it reached 0.28 at 224,101 cycles, at which point the damage jumped to 0.35. This sudden increase in damage is likely the onset of the adhesive failure, which was interrupted by the weld interlocking with the FRP as discussed earlier. The damage then continued to increase at a much more rapid rate until it reached 0.69, when the weld at the end of the diagonal ripped through the FRP composite jacket as shown in Figure 35.

| (a) | (b) |
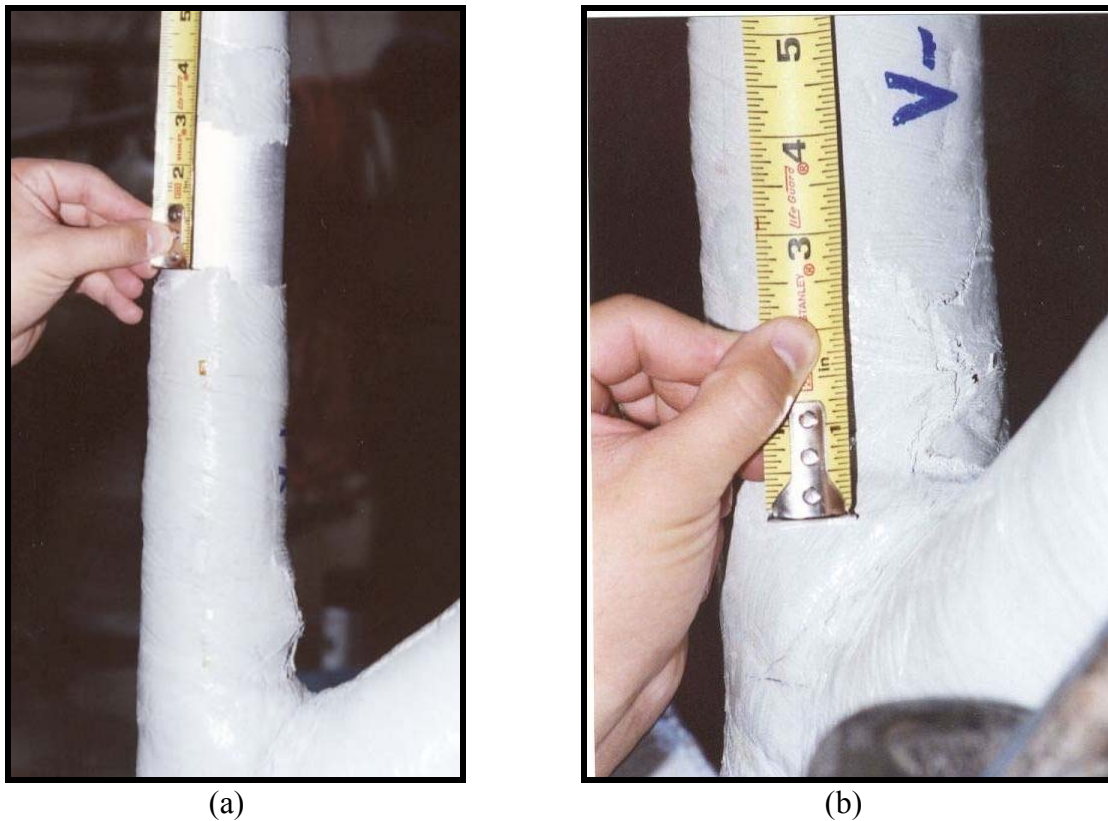
Figure 35. Test V-b (1): (a) Adhesive failure w/FRP tearing, (b) Close-up of FRP tearing failure

40
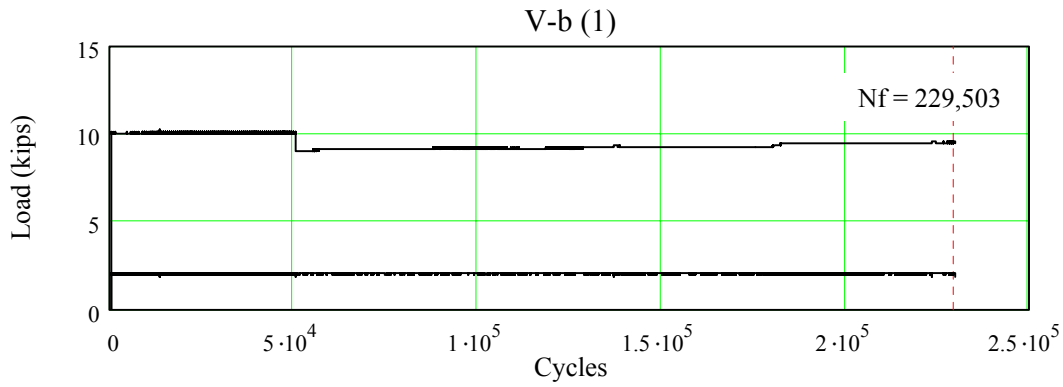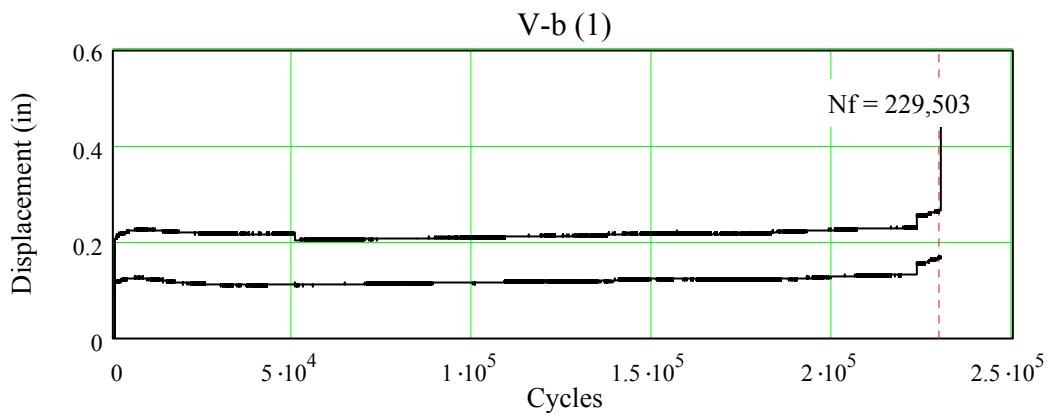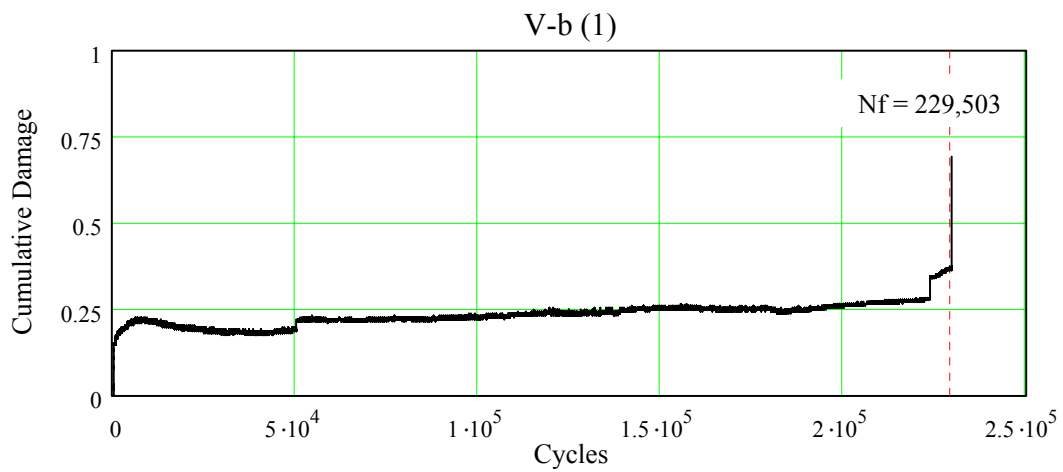
Figure 36. Test V-b (1): (a) Load vs. Cycles, (b) Displacement vs. Cycles, (c) Cumulative Damage vs. Cycles

Failure Mode 2: FRP Composite Tensile Failure

Tests V-c and V-a each failed as a result of FRP composite tensile failure as described in Series (IV) Results, as shown in Figure 37. Test V-c performed much better than the Series (IV) tests at the same load, with 2.5 times more cycles than test IV-a (1) and over 4 times as many cycles as test IV-a (2). However, test V-c still did not perform as well as tests II-a and III-a. Figure 38 shows the load, displacement, and cumulative damage curves for test V-c. Again, from theses plots it can be seen that the failure was rather abrupt, compared to the Series (II) and (III) tests. With a cumulative damage of only 0.12 just prior to failure, it is clear that this failure was abrupt with little or no warning of impending failure, such as large displacements and visually observed cracking.

Test V-a reached the 1×10^6-cycle infinite life benchmark, and was subsequently tested to failure in static tension. It can be seen in Figure 39, that the damage curve is non-uniform with several sudden jumps in damage and displacement. Although these jumps occur at sudden changes in the loading, as shown in Figure 39(a), they are still larger than what might be expected with a small change in the loading. These large jumps in displacement and damage are likely caused by slipping of the gripping mechanism that was used, as described in the previous report (Pantelides and Nadauld 2001). Loading the test unit to 10 kips, and then releasing the load to a minimum tensile load of 1 kip set the gripping mechanism. Unfortunately in this test the load repeatedly dropped below the programmed minimum of 1.2 kips, which may have allowed the gripping mechanism to slip slightly. When the loading was then increased, the gripping mechanism was set again, however at a higher displacement.

Despite these difficulties, it can still be determined from Figure 39 that the cumulative damage, setting aside errors caused by the gripping mechanism, remained fairly constant through the test. The same observations were made in tests II-d, III-c, and III-c, which all reached the 1,000,000 cycle infinite life limit.

The static load vs. displacement curve for test V-a is shown in Figure 40. It can be seen that failure occurred at a load of 25.4 kips. This is near the static tensile capacity of the test unit without undergoing any fatigue cycles, indicating that the composite lost very little of its strength and, therefore, very little damage occurred.

(a)   (b)

Figure 37. FRP Composite Tensile Failure: (a) V-a, (b) V-c
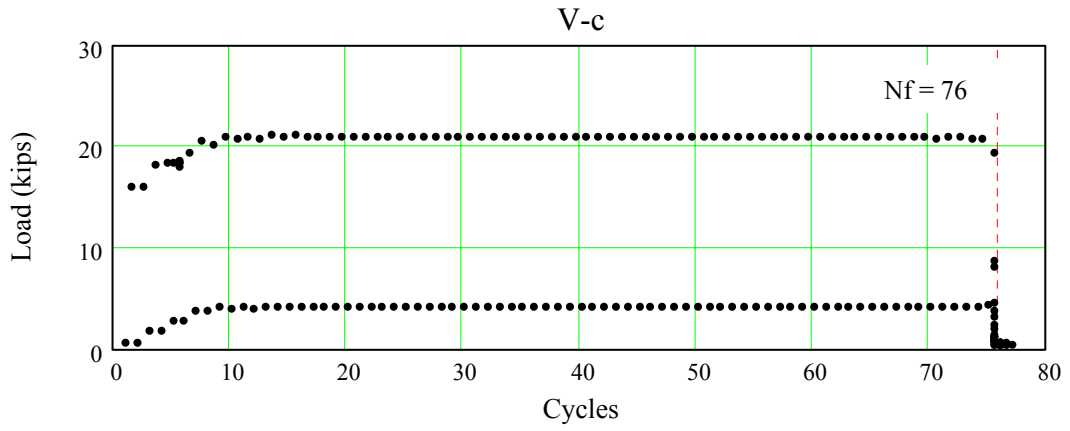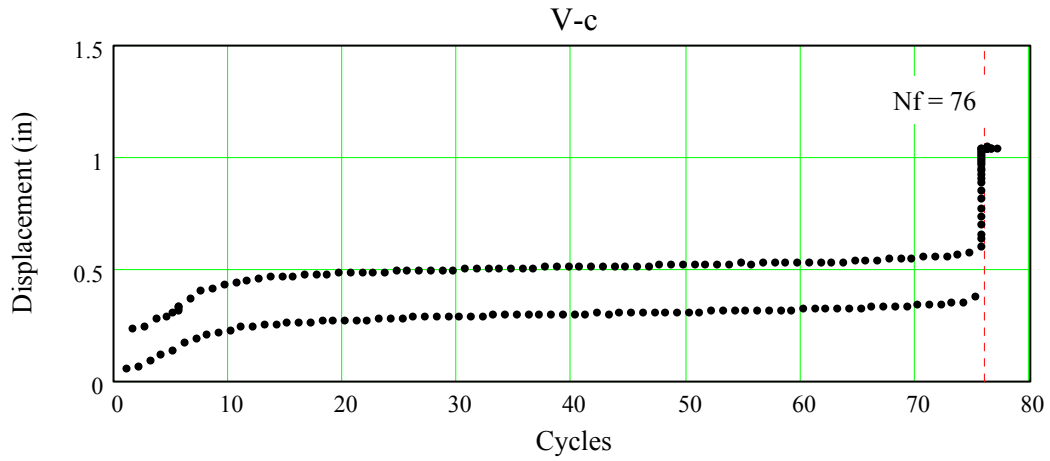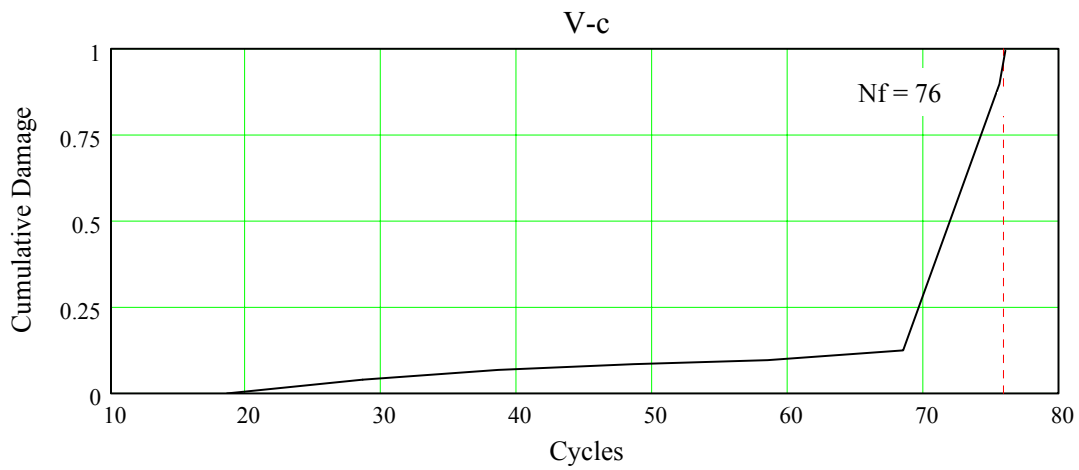
Figure 38. Test V-c: (a) Load vs. Cycles, (b) Displacement vs. Cycles, (c) Cumulative Damage vs. Cycles
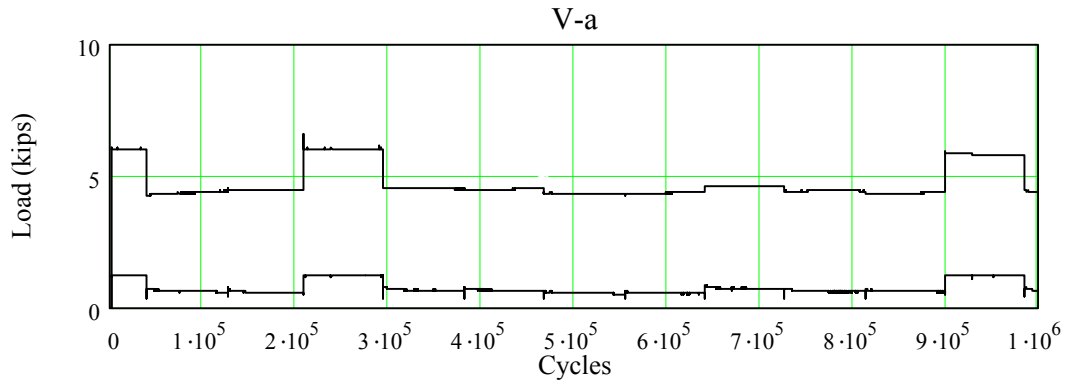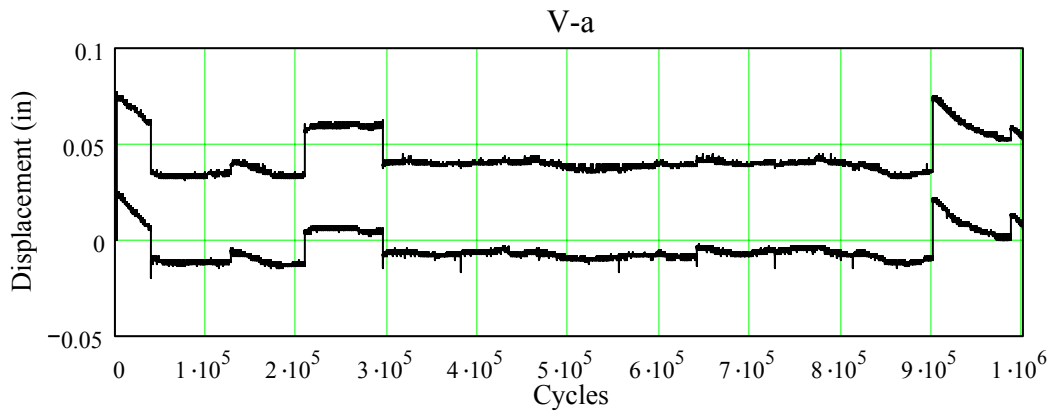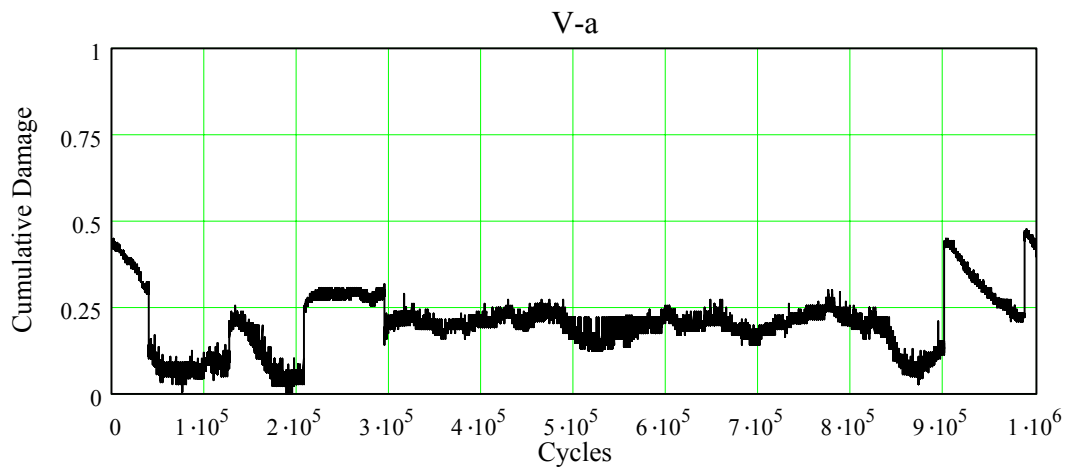
Figure 39. Test V-a: (a) Load vs. Cycles, (b) Displacement vs. Cycles, (c) Cumulative Damage vs. Cycles

44
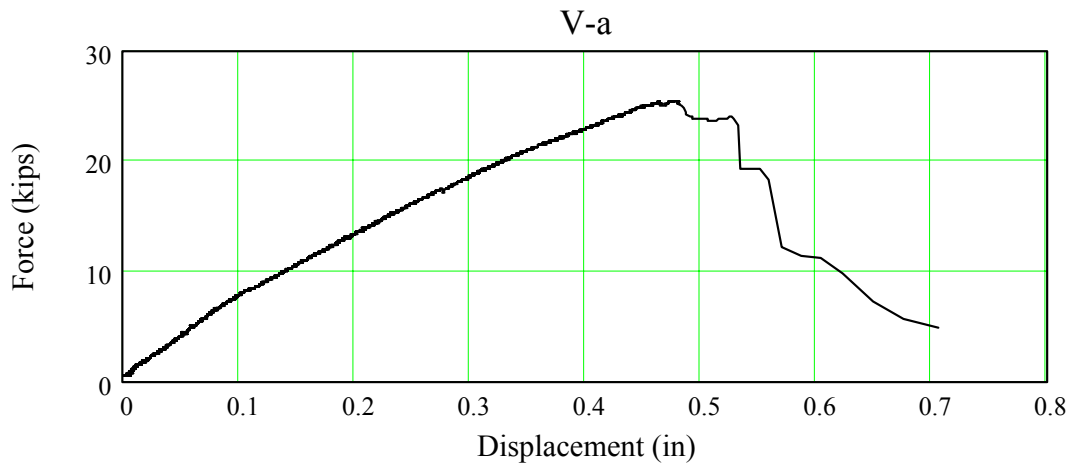
Figure 40. Static Test V-a Load vs. Displacement Curve

Failure Mode 3: FRP Composite Compressive Failure

This failure mode only occurred for one test in all the testing performed in this investigation and the previous investigation (Pantelides and Nadauld 2001), for test V-b (2) as shown in Figure 41. This test was carried out in the same manner as all of the other fatigue tests, and was intended to be a tension only test. However, after 371,100 cycles a power failure occurred and the weight of the actuator caused the test unit to buckle and subsequently fail in combined compression and bending. This test was included in this report due to its good performance up to the power failure, reaching more cycles than test V-b (1) at the same load.

From Figure 42, it can be seen that the cumulative damage increased rapidly at the beginning of the test until at 66,294 cycles, when the damage was 0.35. At this point in the test, two cracks had developed on the FRP, one 2 in. long at the toe of the weld, and another approximately 1.5 in. above the first which was 1 in. long, as shown in Figure 43(a). The cumulative damage then slowly increased until it reached a value of 0.42 at failure. Due to the large amount of damage that had already taken place, it is likely that the test unit was close to failure in tension due to the fatigue loading prior to equipment failure.

(a)   (b)
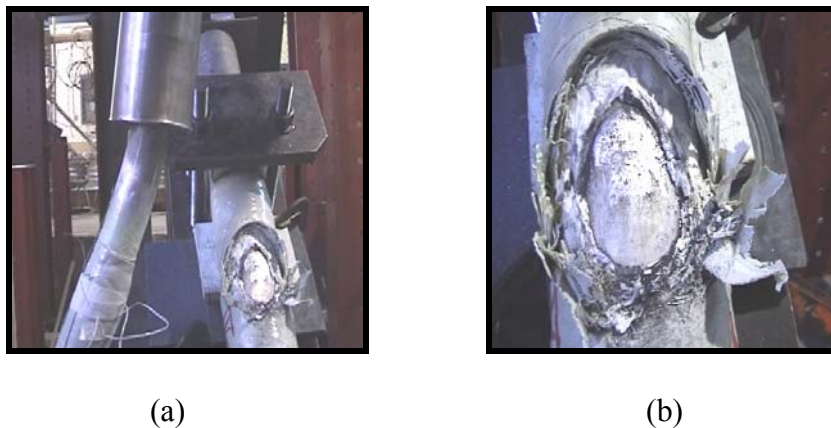
Figure 41. Test V-b (2): (a) Buckled diagonal, (b) Failed FRP at chord

45
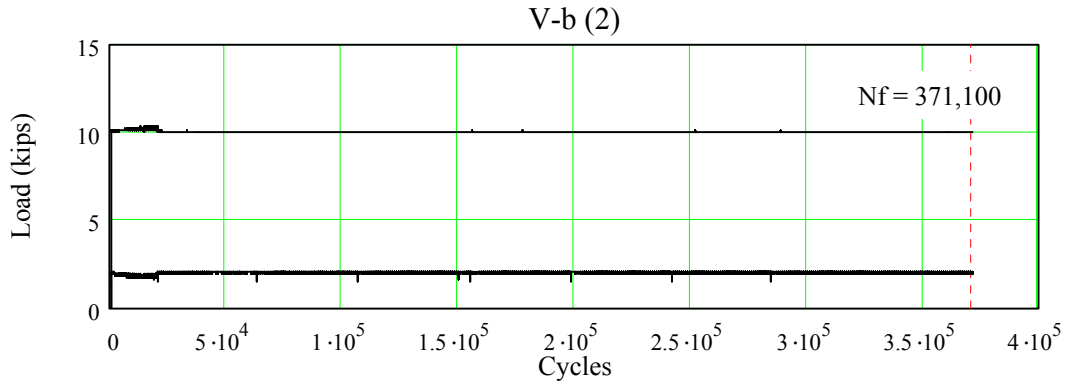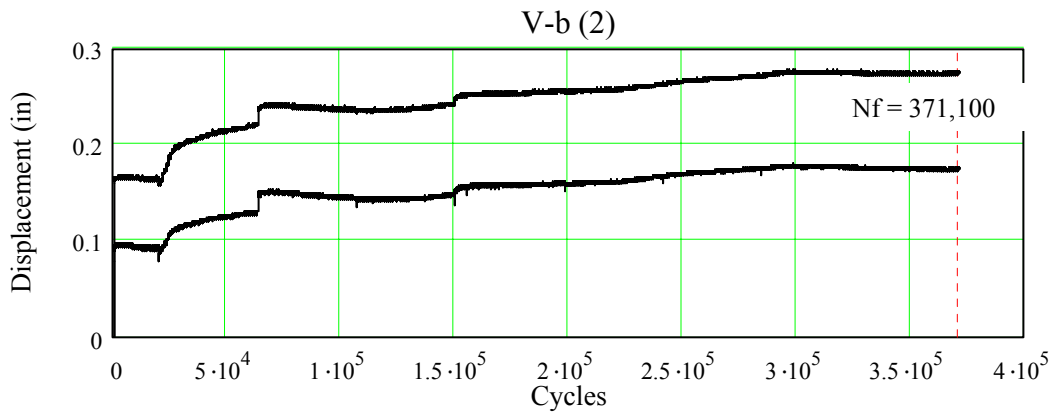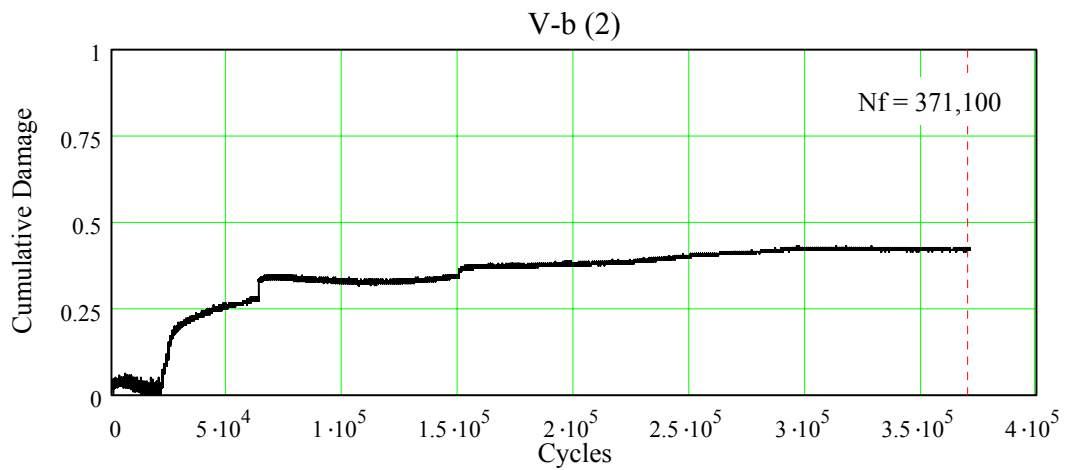
Figure 42. Test V-b (2): (a) Load vs. Cycles, (b) Displacement vs. Cycles, (c) Cumulative Damage vs. Cycles

(a)   (b)

Figure 43. Test V-b (2): (a) cracking at approx. 65,000 cycles, (b) cracking at approx. 290,000 cycles

6. Summary of Experimental Results

A summary of the experimental results for the two static tests, and the four fatigue series is given in Table 7. The static tests show a mean ultimate tensile load of 28.6 kips. This value is slightly higher than the one test carried out in the previous investigation (Pantelides and Nadauld 2001). This is due to the better quality of the welds in the present tests, which was confirmed by observation after completion of the tests.

The results of the four fatigue series are also shown in Table 7. In Series (II), and (III), tests were carried out at 21 kips, 15 kips, 10 kips, and 6 kips maximum load. The stress ratio was approximately 0.20 for all tests (including Series IV and V). In Series (II), for the as-is welded joints, the largest number of cycles experienced was $1\times10^6$ for the 6 kips maximum load. In Series (III), for the retrofitted joints from the field with GFRP composite, the largest number of cycles experienced was 1×10^6 for both the 10 kips and 6 kips maximum loads. In Series (IV), for the tack-welded joints with new aluminum pipes and GFRP composite, tests were carried out at 21 kips, 15 kips, and 10 kips maximum load; the largest number of cycles experienced was 27,115 for the 10 kips maximum load. In Series (V), for the reclaimed aluminum joints with the weld 90% destroyed and retrofitted with GFRP, tests were carried out at 21 kips, 10 kips, and 6 kips maximum load; the largest number of cycles experienced was 1×10^6 for the 6 kips maximum load.

Figure 44 shows the S-N curves for all the fatigue tests. It can be observed that the as-is welded test units (Series II) and the retrofitted joints from the field with GFRP composites (Series III) show similar behavior. The retrofitted units from the field with GFRP composite showed better fatigue behavior for the lower stress range. On the other hand, the tack-welded joints with new aluminum pipes and GFRP composites (Series IV) did not perform as well as Series (II) and (III). This poor performance was due to decreased bond strength caused by the use of new aluminum test units. Finally, the reclaimed aluminum units with the weld 90% destroyed and retrofitted with GFRP (Series V) test units performed better than Series (IV) but not as well as Series (II) and (III) in the high stress range; however, Series (V) did perform as well as Series (II) in the lower stress range as evidenced by Figure 44.

In Figure 44, it should be noted that the lowest stress range of 6 kips is in fact still 1.77 times the Constant Amplitude Fatigue Threshold specified by AASHTO (2001). Given this, and the fact that the as-is welded units (Series II), the retrofitted units from the field with GFRP composites (Series III), and the reclaimed aluminum units with the weld 90% destroyed and retrofitted with GFRP (Series V) reached 1×10^6 cycles, it can be concluded that the retrofit of the aluminum joints with GFRP composites concerning fatigue resistance was successful.

Table 7. Summary of Experimental Results

Series I: Test Results for Static Tests of As-is Welded Aluminum Connections with no visible cracks.

Specimen	Type**	Failure	Maximum Load
I-a*	II	Weld & Base	28.81 kips
I-b*	II	Weld & Base	28.26 kips

Series II: Test Results for Fatigue Tests of As-is Welded Aluminum Connections with no visible cracks.

Specimen	Type**	Failure	Average Maximum Load	R	Cumulative Damage D	Number of Cycles N_f
II-a (1)*	I	Weld	21 kips	0.190	-	5,690
II-a (2)	I	Weld & Base	21 kips	0.190	0.45	14,448
II-b (1)*	II	Weld & Base	15 kips	0.267	0.79	28,491
II-b (2)	II	Weld & Base	15 kips	0.267	0.58	48,096
II-c	II	Weld & Base	10 kips	0.200	0.64	320,829
II-d‡	I	Infinite Life	5.2 kips	0.173	0.22	1×10^6

‡ After 1×10^6 cycles the static tensile load capacity was = 22.2 kips.

Series III: Test Results for Fatigue Tests of Cracked Aluminum Connections from the field retrofitted with GRRP.

Specimen	Type**	Failure	Average Maximum Load	R	Cumulative Damage D	Number of Cycles N_f
III-a	II	Weld, Base, & FRP	21 kips	0.19	0.33	6,763
III-b	I	Weld, Base, & FRP	15 kips	0.267	0.79	69,194
III-c+	II	Infinite Life	10 kips	0.200	0.36	1×10^6
III-d++	II	Infinite Life	4.8 kips	0.135	0.19	1×10^6

+After 1×10^6 cycles the static tensile load capacity was = 20.9 kips
++After 1×10^6 cycles the static tensile load capacity was = 44.2 kips

Series IV: Test Results for Fatigue Tests of Tack-welded Aluminum Connections Retrofitted with GFRP.

Specimen	Type**	Failure	Average Maximum Load	R	Cumulative Damage D	Number of Cycles N_f
IV-a (1)	I	Adhesive	21 kips	0.19	-	16
IV-a (2)	I	FRP	21 kips	0.20	-	29
IV-b	I	FRP	15 kips	0.20	0.33	913
IV-c	I	Adhesive	10 kips	0.20	0.23	27,115

Series V: Test Results for Fatigue Tests of Reclaimed Aluminum Connections with the weld 90% destroyed Retrofitted with GFRP.

Specimen	Type**	Failure	Average Maximum Load	R	Cumulative Damage D	Number of Cycles N_f
V-a[+]	II	Infinite Life	6 kips	0.156	0.47	1×10^6
V-b (1)	II	Adhesive	10 kips	0.20	0.35	229,503
V-b (2)	II	FRP	10 kips	0.20	0.42	371,100[†]
V-c	II	FRP	21 kips	0.20	0.13	76

[+]After 1×10^6 cycles the static tensile load capacity was = 25.4 kips.
[†]Failed in compression due to power outage.

* = No pipe in the chord
**** = Refers to size of the specimen, see Table 1**
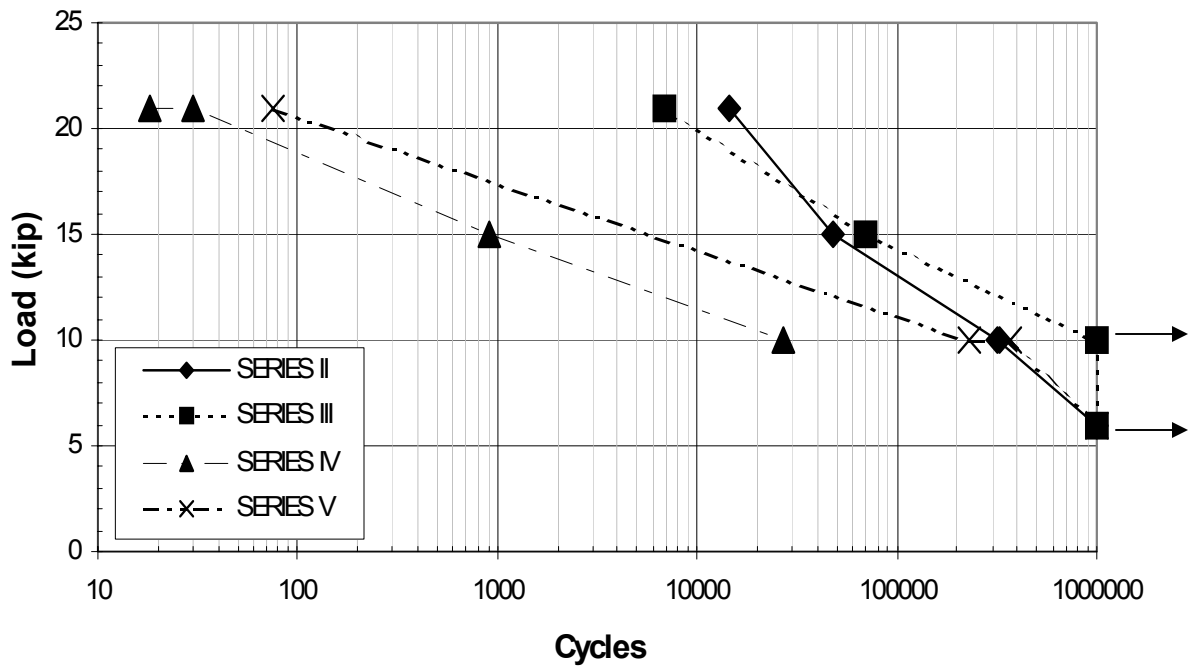
Figure 44. S-N Curves

7. Analytical Model

Technique and Results

To better understand the effects of retrofitting aluminum trusses with FRP composites, an analytical model was developed using SAP2000 (CSI 1997). The objective for creating the model was to determine the effect of cracks in the weld between the diagonal and the chord, and also the effect of repairing the cracked joints using GFRP composites. The model was created for the sign structure shown in Figure 3. The chord and diagonal were modeled using the sizes for a Type I connection as shown in Table 1. The steel tube columns were modeled as 18 in. outside diameter with a 0.465 in. thick wall. The footing behavior was not modeled, and the steel tube columns were considered fixed at the base.

Three different scenarios were analyzed: 1) the sign structure as-is, with no cracks, 2) the sign structure with seven cracked welds, four in the vertical plane and three in the bottom inclined plane, and 3) the same seven cracked welds in Scenario 2, retrofitted with the GFRP composite. For each scenario, the mode shapes, periods, horizontal stiffness, and vertical stiffness were determined. The mode shapes and periods were determined using an eigenvector solution, with zero damping. The horizontal stiffness was determined by applying a horizontal load at the mid-span of the truss with a unit load of 1 kip. The displacement at mid-span due to the 1 kip horizontal load was determined using SAP2000. The truss stiffness could then be determined by dividing the 1 kip load by the displacement obtained in the model. The vertical stiffness was obtained in a similar manner, except that the 1 kip load was placed in the vertical direction and was divided by the vertical displacement at mid-span.

In Scenario 1, all of the diagonal-to-chord connections were modeled using linear spring elements, with stiffness in the axial direction of 41.7 kips/in. This stiffness was determined from static test results of the as-is connection. The stiffness was calculated by dividing the peak load by the displacement at peak load. The first five periods, the vertical and horizontal stiffness, and the first five mode shapes for Scenario 1 are shown in Table 8 and Figure 45.

In Scenario 2 all of the un-cracked diagonal-to-chord connections were modeled as discussed in Scenario 1. The cracked connections were simply modeled as disconnected, with no resistance at the chord–diagonal interface. This is a severe case, where the connection is completely gone. The seven cracked joints were selected at the bottom chord at mid-span and extending three joints to either side of mid-span. At each K connection only one of the diagonal-chord connections were modeled as cracked, with the other connection modeled intact as described in Scenario 1. The seven cracked welds represent 6.5% of all of the connections on the entire sign structure. The results for relevant modes and the vertical and horizontal stiffness are shown in Table 8. The first 14 modes consisted of only the severed diagonal elements, and therefore had very little participation to the entire structural response. All of these modes had a frequency near 2 Hz, plus or minus 0.1 Hz. The 16th mode had a period of 0.302 seconds, which is close to the 1st mode period of Scenario 1 of 0.300 seconds; the 19th mode had a period of 0.212 seconds, which was close to the 2nd mode period of Scenario 1 of 0.213 seconds. The 16th mode shape of Scenario 2 is shown in Figure 46, which demonstrates that the predominant motion is similar to the 1st mode of Scenario 1.

In Scenario 3, all of the un-cracked diagonal-to-chord connections were modeled similar to Scenario 1 but with a reduced stiffness. The cracked connections were assumed as retrofitted with GFRP composites, and were modeled using linear link elements with stiffness in the axial direction of 29.1 kips/in. This stiffness was determined from static test results of the retrofitted

connection with the weld completely severed and retrofitted with GFRP composites (Pantelides and Nadauld 2001). An average value of the experimental stiffnesses was used. The first five periods and the vertical and horizontal stiffness are shown in Table 8. The first five mode shapes were similar to the mode shapes for Scenario 1, as shown in Figure 45.

Table 8. Analytical Model Results

	Scenario 1	Scenario 2	Scenario 3
Horizontal Stiffness (kips/in)	0.939	0.568	0.935
Vertical Stiffness (kips/in)	1.424	0.291	1.384
Mode 1 Period (sec.)	0.300	0.526	0.300
Mode 2 Period (sec.)	0.213	0.514	0.213
Mode 3 Period (sec.)	0.195	0.513	0.195
Mode 4 Period (sec.)	0.185	0.511	0.186
Mode 5 Period (sec.)	0.183	0.511	0.184

(a) Mode 1   (b) Mode 2   (c) Mode 3

(d) Mode 4   (e) Mode 5
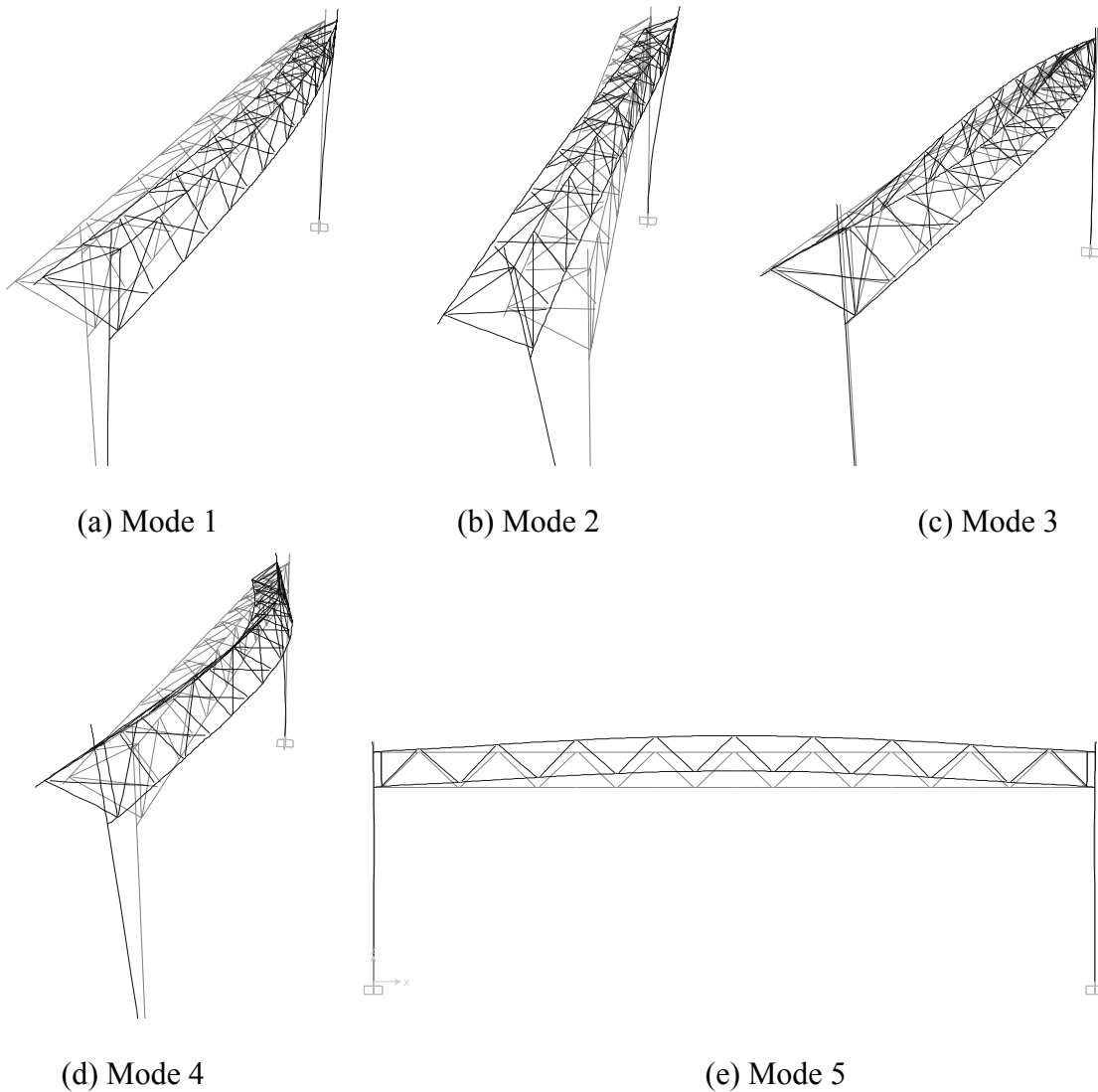
Figure 45. Scenario 1 and Scenario 3 mode shapes
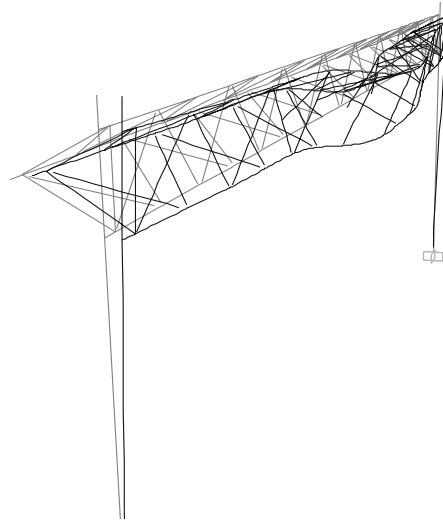
Figure 46. Mode shape 16 for Scenario 2

Discussion

      Scenario 1, the as-is model, serves as the baseline for all of the other results. As expected, in Scenario 2, both the horizontal and vertical stiffness of the structure were significantly reduced, with the vertical stiffness being the most severely influenced (20% of as-is). The mode shapes and periods also changed dramatically in Scenario 2, as indicated by comparison of Figures 45 and 46. Clearly Scenario 2 is a severe case that would result in severe damage and/or collapse of the sign structure.

      In Scenario 3, the horizontal and vertical stiffness of the structure were only slightly reduced and the mode shapes and periods were essentially identical (vertical stiffness was 97% of the as-is). This indicates that use of the GFRP composite to retrofit the truss would have only a small influence on the performance of the sign structure, even though the stiffness of the joints was reduced from 41.7 kips/in. to 29.1 kips/in.

8. Conclusions and Recommendations

The static tests, Series (I), performed as expected but with a higher ultimate load than the previous study by a factor of 1.16; this is attributed to the better quality of the welds in the test units used for the static tests. The failure mode for both static tests was due to a crack initiating at the toe of the weld and continuing almost entirely around the chord.

For the fatigue portion of this study, each series exhibited its own failure mode; in some cases more than one failure mode was experienced within the same series. In Series (II), for the as-is welded joints, a single failure mode was experienced. The failure mode started with a crack at the toe of the weld, and then the crack propagated into the base material of the chord.

In Series (III), for the repaired joints from the field with GFRP composites, two distinct failure modes were observed. Failure Mode 1 was due to weld throat cracking and subsequent FRP composite tensile failure. Failure Mode 2 was due to cracking at the toe of the weld followed by cracking of the throat of the weld, and subsequent FRP composite tensile failure. Overall, Series (III) performed better than Series (II) especially at the lower stress range.

In Series (IV), for the tack-welded joints with new aluminum pipes and GFRP composite, two distinct failure modes were observed. The first failure mode was an adhesive failure in which the diagonal brace pulled out of the FRP composite at lower strains than ultimate of the FRP composite. The second failure mode was tensile failure of the FRP composite, in which the FRP composite achieved a high percentage of its ultimate strength. After completion of the tests, it was determined that the performance of the Series (IV) tests was due in part to poor bond between the aluminum and the FRP. Series (IV) test units were constructed of new aluminum pipes; as such, the aluminum surface contained oils and other elements that were not completely removed in the preparation steps outlined in the first report (Pantelides and Nadauld 2001). Also, because the aluminum pipes were new, their surface had not oxidized. It has been documented that the bond between aluminum and FRP is significantly increased when the aluminum surface has been oxidized.

In Series (V), for the reclaimed aluminum units with the weld 90% destroyed and retrofitted with GFRP composite, two failure modes were observed. The first failure mode was an adhesive failure with FRP tearing. The second failure mode was FRP composite tensile failure. Series (V) performed as well as Series (II) for the as-is welded joints in the lower stress range. Bearing in mind that the lowest stress range of 6 kips is in fact still 1.77 times the Constant Amplitude Fatigue Threshold specified by AASHTO (2001), this result is deemed satisfactory.

From analytical results of a typical sign truss structure with seven connections severely cracked, which is 6.5% of all of the connections on the entire sign structure, both the horizontal and vertical stiffness of the structure are significantly reduced, with the vertical stiffness being the most severely influenced (20% of as-is); the mode shapes and periods also change dramatically. However, when the severely cracked connections are repaired with GFRP composites, the horizontal and vertical stiffness of the structure is only slightly reduced and the mode shapes and periods are essentially identical (vertical stiffness was 97% of as-is), even though the stiffness of the damaged joints with GFRP composites was only 70% of the original undamaged joint. This indicates that the use of GFRP composites to retrofit the truss would have negligible influence on the performance of the sign structure.

From the experimental results of this study, as well as that of the previous study (Pantelides and Nadauld 2001), it is recommended that to avoid adhesive failures, the minimum bond length should be 18 in. on the diagonal. This is not believed to add appreciable cost to the repair, and is good insurance against brittle failures without warning.

Surface preparation procedures are critical for desirable performance. It was observed in these tests that the tubular surface of older structures, that have been in service for many years, was sufficiently roughened and performed better in terms of bond compared to new aluminum tubes. According to the literature, the exposure to the elements during which roughening and discoloration reach satisfactory levels for proper bond is between 6 to 36 months of service, depending on the environment. Caution should be used for performing the repair on brand new aluminum structures, which should have more rigorous surface preparation procedures than the ones described in these tests. In addition, the bond length might have to be increased beyond the recommended 18 in. for satisfactory performance.

It can be concluded that for the 6 kips stress range, the performance of Series (III) for the repaired joints from the field with GFRP composites is better than Series (II) for the as-is welded joints; the performance of Series (V) for the reclaimed aluminum units with the weld 90% destroyed and retrofitted with GFRP composites is as good as Series (II) for the as-is welded joints. Thus, the fatigue test results agree with the results of the static tests (Pantelides and Nadauld 2001), i.e. that the GFRP repaired connections behave as well as the uncracked aluminum connections for the range of loading expected in service; therefore, the repair technique with GFRP composites is adequate and can be used in construction.

9. References

Aluminum Association Inc. (1986). *Aluminum Construction Manual*, Section 1 – Specifications for Aluminum Structures, 5th Ed., Washington, D.C.

American Association of State Highway and Transportation Officials (1975). *Standard Specifications for Structural Supports for Highway Signs, Luminaires and Traffic Signals*. AASHTO Subcommittee on Bridges and Structures, Washington, D.C.

American Association of State Highway and Transportation Officials (1998). *LRFD Bridge Design Specifications, SI Units – Second Edition*, Washington, D.C.

American Association of State Highway and Transportation Officials (2001). *Standard Specifications for Structural Supports for Highway Signs, Luminaires and Traffic Signals*. 4th Edition, Washington, D.C.

Bull, J.W. (1994). *The Practical Design of Structural Elements in Aluminium.* Ashgate Publishing Company, Brookfield, Vermont.

Computers and Structures, Inc. (1997). *SAP2000 Analysis Reference*, Vol. I, Berkeley, California.

Dwight, J. (1999). *Aluminium Design and Construction.* E & FN Spon, London.

Kaczinski, M.R., Dexter, R.J., and Van Dien, J.P. (1998). *NCHRP Report 412: Fatigue-Resistant Design of Cantilevered Signal, Sign, and Light Supports,* Transportation Research Board, National Research Council, Washington, D.C.

Pantelides, C.P., and Nadauld, J. (2001). "Repair of cracked aluminum overhead sign structures with fiber reinforced polymer composites." *Research Report CVEEN-01/01,* Dept. of Civil & Environmental Engineering, Univ. of Utah, Salt Lake City, Utah.

Sharp, M.L. (1993). *Behavior and Design of Aluminum Structures.* McGraw-Hill, New York, New York.

Sharp, M.L., Nordmark, G.E., and Menzemer, C.G. (1996). *Fatigue Design of Aluminum Components and Structures.* McGraw-Hill, New York, New York.